1D INVERSION OF MAGNETOTELLURIC DATA FROM ASHUTE, BUTAJIRA GEOTHERMAL PROSPECT, SE-ETHIOPIA AND ITS GEOTHERMAL IMPLICATIONS

Tsegaye Wondifra Tadesse
Geological Survey of Ethiopia (GSE)
Geothermal Resource Exploration and Evaluation Directorate
P.O. Box 2302
Addis Ababa
ETHIOPIA
josywondifra@gmail.com

ABSTRACT

Geophysical surveying is an important part in exploration of geothermal energy. A magnetotelluric (MT) survey was conducted in the Ashute, Butajira geothermal prospect in SE-Ethiopia, where 28 soundings were carried out in 2017. In this project, the 28 MT soundings have been processed and 1D inverted. The results are presented here as resistivity cross-sections and depth-slices, and compared to previous geological findings.

The Ashute area is characterized by a conductive shallow layer with resistivity values less than 10 Ωm and an average thickness of about 1,600 m. It reaches down to a depth of 200 m a.sl. The subsurface is composed of volcanic sediments including lithified ash, fine- to coarse-grained sandstone, well laminated conglomerate and debris or lahar. The clasts mostly consist of pyroclastic material derived from a silicic centre from the south. They can be correlated with sediments at shallow depth and the low-resistivity layer. Below the low-resistivity layer there is high resistivity with resistivity values greater than 70 Ωm. This layer is probably related to the basement, fractured basalt and scoria.

The high-resistivity layer below the conductive zone is believed to reflect major fault systems, the tectonic trend of the Debre zait Selti rift graben and the Main Ethiopian Rift (MER). Geothermal fluid at depth emerges to shallow level most likely along a NE-SW discontinuity and NW-SE structures. It flows laterally and enriches the shallow permeable formation, and appears as thermal manifestations in the field. Strike analyses for different frequencies (depth levels) indicate a general NE-SW geo-electrical strike direction for shallow depths which coincides with the major trend of the western rift axis. At greater depths the geo-electrical structure changes.

In further studies of the area, it is recommended to add MT and co-located TEM soundings towards the north and west of the Ashute field to define the resistivity structure better, as well as performing TEM soundings at the same location as the already existing MT sites to correct for the static shift of the MT data. Finally, detailed geological mapping of the area is proposed, in particular tectonic mapping, and gravity surveying to delineate geological structures.

1. INTRODUCTION

Exploration for geothermal resources in Ethiopia close to the rift margin has been carried out since the 1970s. Regional exploration activities have been done by both national and international organizations. Geological surveys have been performed for the whole rift at a scale of 1:500,000. Geological, geochemical and airborne geophysical results have identified 16 geothermal prospect areas in the rift. Later, additional explorations were conducted and currently the prospect areas are around 24, and the estimated potential more than 10,000 MWe.

The Butajira Selti prospect area is on the western fault border of the rift axis. Previously, geothermal exploration was focused on the axis and the eastern part of the active fault system of the Main Ethiopia Rift (MER), particularly on the Wonji fault system in both the southern and northern Afar rift. The project area (Figure 1) was recommended in the United Nation Development Programme technical report for further detailed geological and geochemical study (UNDP, 1973). The area was regarded as a low-enthalpy geothermal resource which could be used for direct use rather than electrical generation. In April 2014 a sudden explosion of hot thermal fluid occurred during deep drilling of an irrigation well. This potentially hazardous situation changed previous views about the area and required detailed exploration work.

The Ashute, Butajira geothermal project work started with geological, geophysical and geochemical surveying in March, 2017. Geophysical survey using resistivity and magnetic methods in Ashute area was performed from April 10th, 2017 to May 27th, 2017. The resistivity survey in the project area was not completed. However, these studies provided valuable information about the shallow and deep lying resistivity structure of the area. The future plan is to add several MT and TEM stations through a joint and integrated scientific study by Geological Survey of Ethiopia (GSE) and Japan International Cooperative Agency (JICA). Results from MT surveys indicate that there are many unexpected
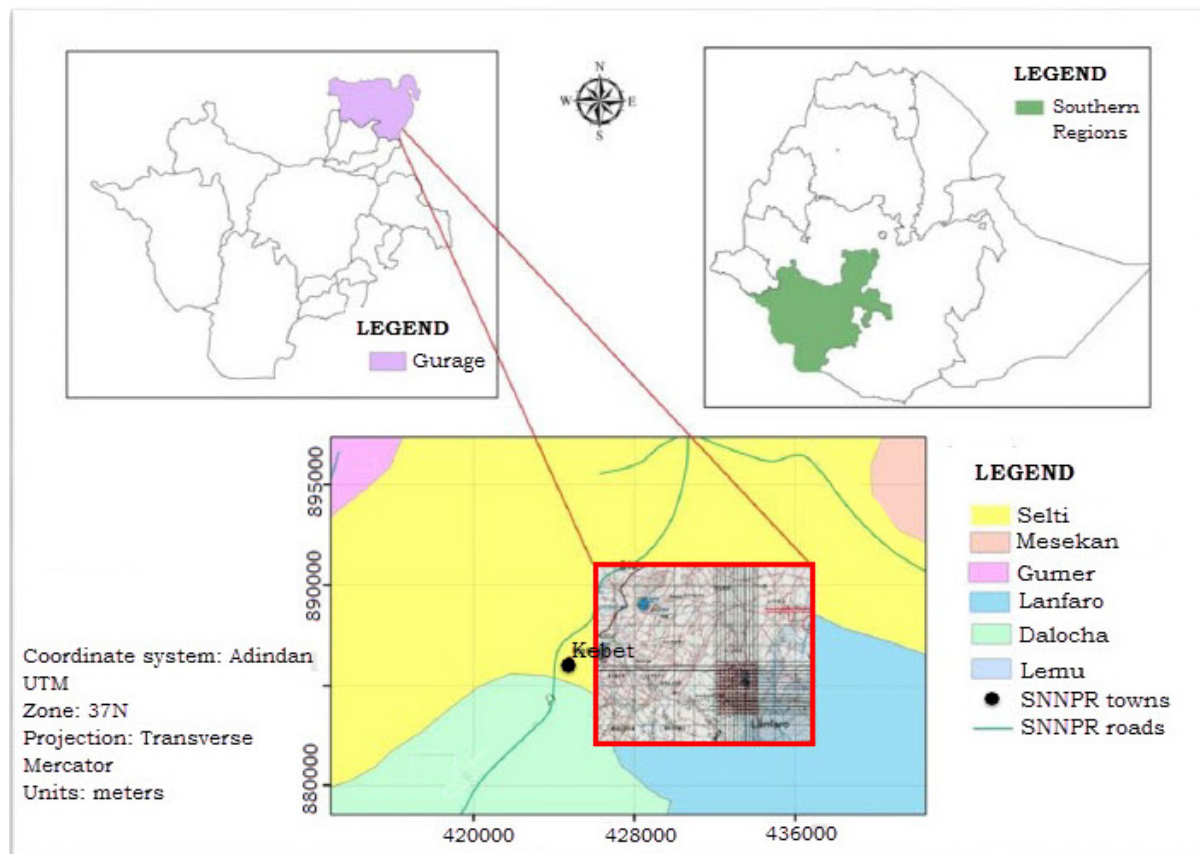
FIGURE 1: Location and accessibility of the project area in Ethiopia (Gebrewold, 2017)

resistivity anomalies in the area and therefore, Selti Woreda (including Ashute) was selected for further exploration. The main geothermal manifestations are mud pools, hot springs, fumaroles and geothermal grassland. Resistivity surveying had not been done previously in the area, only regional gravity and magnetic data exist.

The Ashute, Butajira geothermal field is located in the Southern Nations Nationalities Regional State, in the south-western part of the Western margin of the Main Ethiopian Rift, about 150 km southeast of Addis Ababa in the low plain of the Ethiopian Rift (Figures 1 and 2). The nearby towns are Butajira and Kebet in Selti Wereda. The prospect area lies within two zones of the state administration, Gurage and Selti. Its boundaries are 8° 08' 32.9" N to 7° 51' 42.8" N and 38° 13' 10.7" E to 38° 32' 13.9653" E. The highway from Addis Ababa to Hosanna in the west vicinity of Garage highland runs in the northeast direction in the low plain of the rift valley. There is a gravel road from Kebet Selti Wereda to the Ashute prospect area. The weather is generally dry.
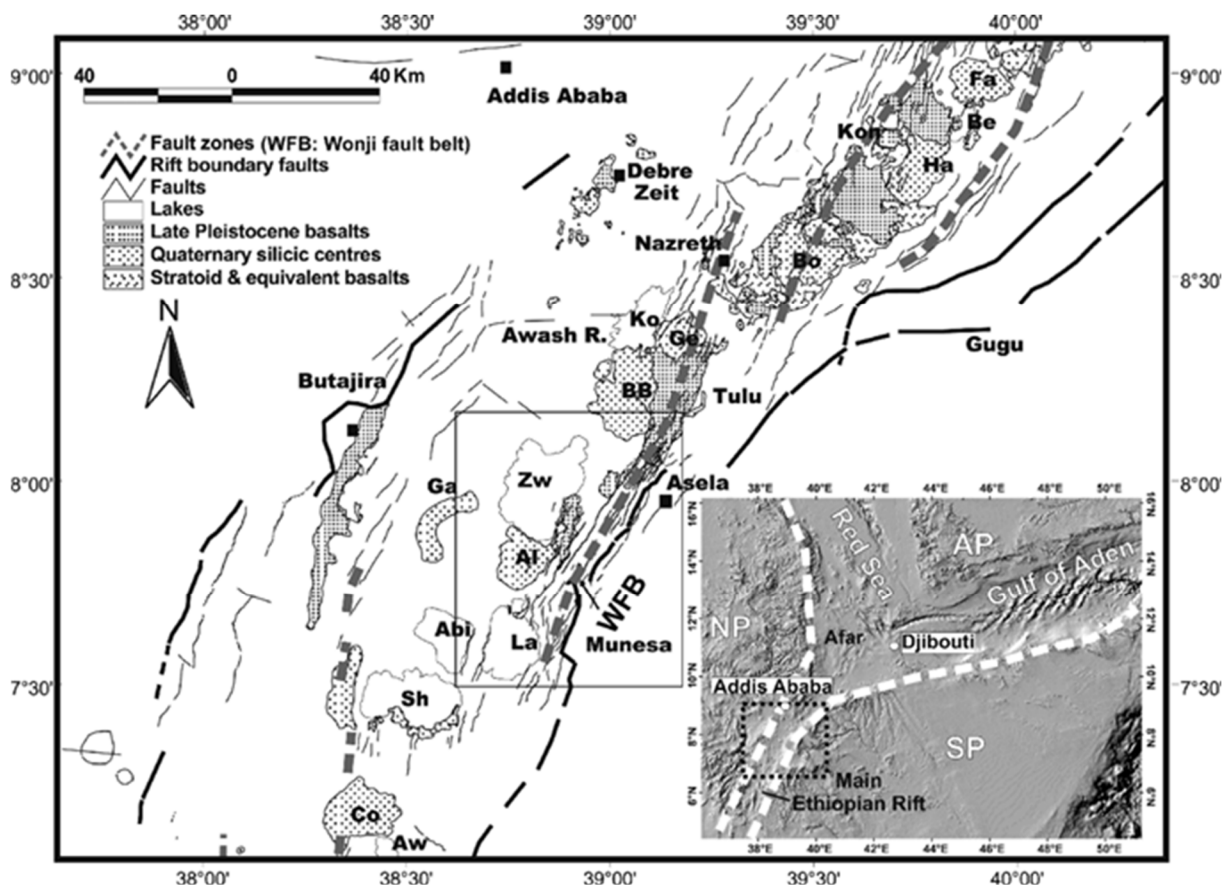
FIGURE 2: Structural map of the northern sector of the Main Ethiopian Rift (MER) and major faults. The study area is within the rectangle. Trend of fault zones includes the WFB which in the study area constitutes the eastern side of the MER Lakes. The inset map shows the plate tectonics of the Afar triple junction. Dashed rectangle in the smaller map, shows location of the structural map. Lakes: Aw: Awasa; S: Shala; Abi: Abijata: La: Langano; Zw: Zway; Ko: Koka; Be: Beseka. Volcanoes: Co: Corbetti; Ga: Gademota; Al: Aluto; BB: Bora Bericcio, Ge: Gedemsa; Bo: Bosetti; Ha: Hada; Kon: Kone; Fa: Fantale. NP: Nubian plate; SP: Somalian plate; AP: Arabian plate (Pizzi et al., 2006)

2. THE GEOLOGY OF THE STUDY AREA

The Main Ethiopian Rift (MER) is the northern part of the East African Rift System (EARS) (Figures 2 and 3). There different volcanism (mainly composition and volumes) as a function of the extension along the rift margin can be studied. As stated by Abebe and Alem (2007) and Pizzi et al. (2006), the composition of the erupted material along the MER can be divided into two categories. The northern most part is characterized by basaltic lava flows, connected with a flat area of volcanoes and eruptive fissures (see, e.g. Hayward and Ebinger, 1996; Lahitte et al., 2003). In contrast, the central and southern part of the rift are home of felsic central volcanoes, typically characterized by calderas, associated with
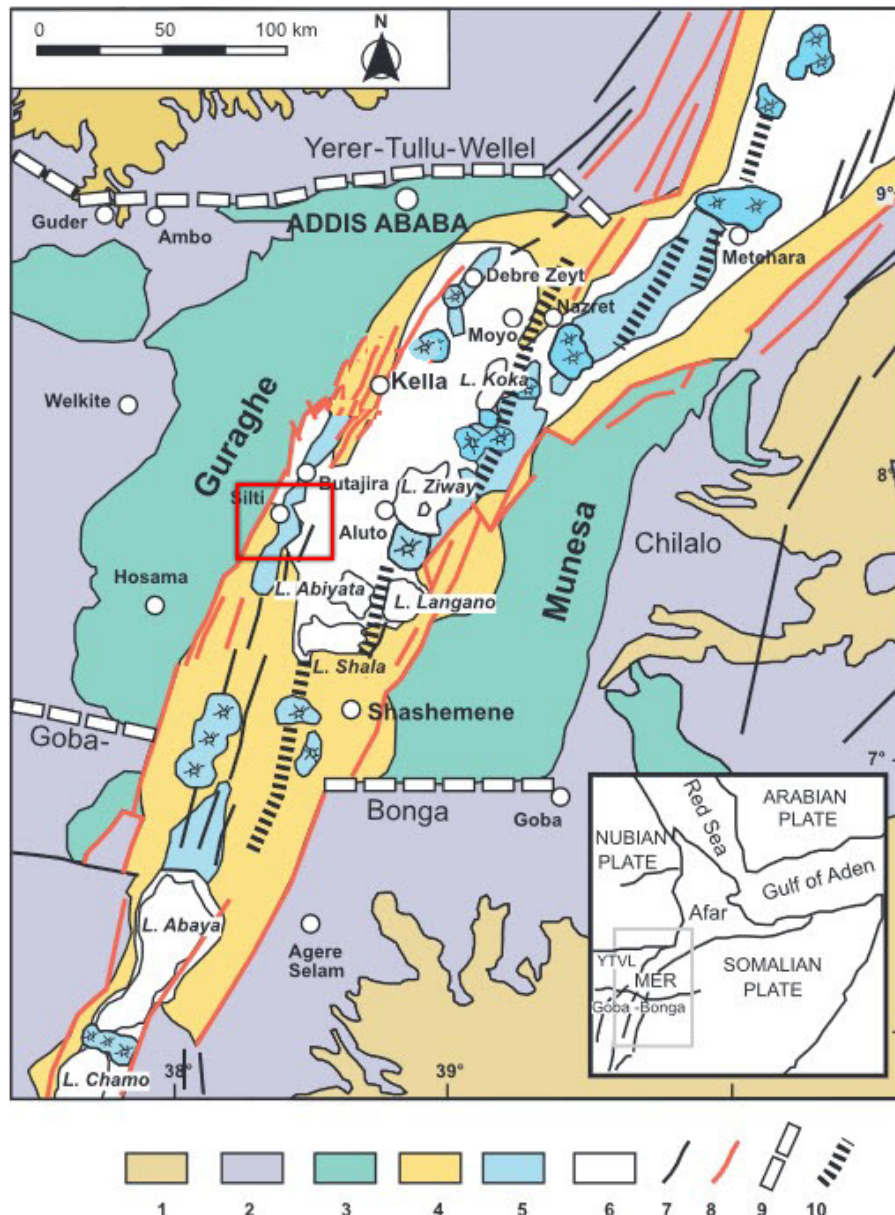
FIGURE 3: Geological map of Central Main Ethiopia Rift (modified from Abebe et al., 2010).
(1) Pre-Tertiary sediments and crystalline basement, (2) Oligocene (32–29 Ma) and lower Miocene
(12–8 Ma) plateau volcanism, (3) Miocene–Pliocene rift-shoulder trachytic-rhyolite volcanic and
pyroclastic layers, (4) Plio-Pleistocene rift floor, (5) Quaternary central volcanic and basaltic lava
flows, and associated scoria cones and phreato-magmatic deposits, (6) Quaternary lacustrine
sediments and interbedded pyroclastics, (7) faults, (8) major rift border faults, (9) major transversal
tectonic lineaments in the basement, (10) Wonji Fault Belt segments;
the red square denotes the boundary of the study area

the release of rhyolite and ignimbrites (e.g. Woldegabriel et al., 1990; Chernet et al., 1998; Ebinger and Casey, 2001; Acocella et al., 2003). This accumulation of volcanic materials is usually interlaid with sedimentary rift deposits (Le Turdu et al., 1999). According to Mohr (1962) the general Quaternary volcano-tectonic setting of the MER is described as an overlapping spreading centre where the Wonji Fault Belt (WFB) is the eastern limb. These NNE-SSW Quaternary rift zones of the WFB form areas of active deformation of a fault which has both horizontal and vertical elements of displacement of the rift floor of the MER (Figure 2).

The second line of a relatively wide planar opening in the bedrock that originated as a fracture of fault and basaltic volcanism is found close to the western escarpment in the central and northern MER. This SSW–NNE line of Quaternary extension (Butajira Selti line of extension) extends as far north as the Quaternary basaltic fields in the Debre Zeit area (Chernet et al., 1998). The Butajira and Debre Zeit Selti volcanic fields are located within the western margin of the MER and formally establish the off-axis belts of Quaternary activity.

Four different major volcanic episodes in the central MER have been identified by various authors (e.g. Abebe et al., 2005; Bonini et al., 2005). A major volcanic episode occurred around 32–29 Ma and covers the main parts of the Ethiopian plateau volcanics as a part of the Trap Series (Hofmann et al., 1997; Pik et al., 1998; Ukstins et al., 2002). Another, less voluminous and more local, volcanic episode (11–8 Ma) was associated with the build-up of a shield volcano with a very broad gently sloping dome, built by flows of very fluid basaltic lava or basaltic–trachytic lava flows. The third episode (5-3 Ma) was characterized by layers of pyroclastic rocks associated with trachytic and rhyolitic lava domes and flows from a few significant central volcanoes, that are located in the MER valley floor and slopes. The latest volcanic episode (<3 Ma) is composed of uncompact pumice fall and flow deposits, rhyolitic–trachytic lava flows from basic central volcanic edifices, fissural basaltic lava flows with connected scoria and phreatomagmatic cones and interbedded layers of rock lying between or alternating with beds of a different kind of rock and lacustrine deposits (e.g. Di Paola, 1976; Seifemichael and Kazmin, 1978; Kazmin et al., 1980; Bigazzi et al., 1993).

Both silicic and basaltic rocks are found in the study area (Figure 4). The compositional variation in the
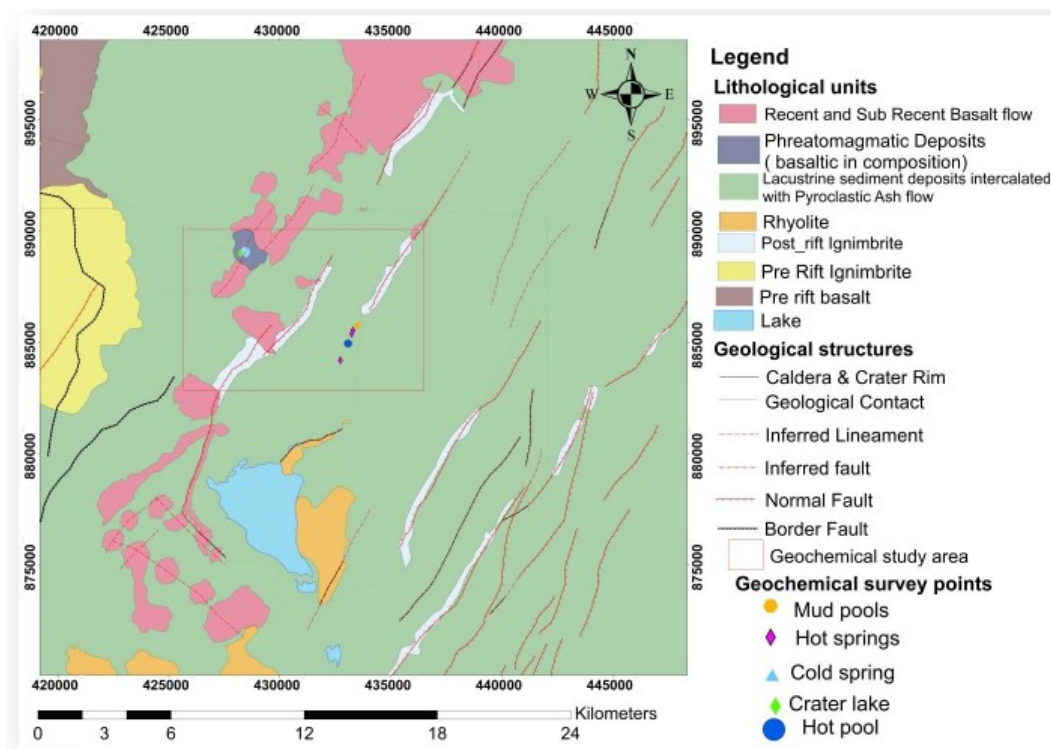
FIGURE 4: Geological map of the study area (modified from Abebe et al., 2017)

rock units is due to volcanism in the MER and is described by a two peaked basalt-rhyolite group (Abebe and Alemu, 2007). The lithological units are scoria (defining lithology for volcanic centres (scoria cones) in the study area), highly vesicular basalt, igneous rock containing abundant vesicles, layered pumice, and pyroclastic flow deposits with strong variations in textural features (porphyritic to a pyritic type). Table 1 lists the rock units in the area. The rocks are strongly weathered and overlain with soil as thick as 0.5 m. Crystalline ignimbrite (containing xenolith of basalt and rhyolite) and lacustrine sediment deposits (lake deposits of sandstone and conglomerate) are also observed.

TABLE 1: Documentation of the rock units in the study area

Date	Site name	Sample code	Rock unit	Remarks
15/2/17	Ashute	0.01	Highly vesicular basalt	—
21/2/17	Har Shetan	0.02	Vesicular basalt	Volcanic crater lake in which basalt is intensively weathered from bottom to top of the crater.
22/2/17	Ashute	0.03	Lacustrine sediment deposits	The area is covered with high grass and characterized by an altered ground of calcium carbonate deposits.
26/2/17	Ashute	0.04	Lacustrine sediment deposits	Very hot pool smelling of H_2S.
04/3/17	Ashute Burako	0.05	Volcanic sediment deposits	The hot spring is found to be a source for a traditional swimming pool close to the place.
06/3/17	Balew Keriso	0.06	Basalt	—

2.1 The general geological and tectonic settings of the Ethiopia Rift System

The MER is an approximately NE trending sector of the East African Rift system that contains a series of rift segments that increase in size from the Afar Triple Junction (at the Red Sea-Gulf of Aden intersection) to the Kenya Rift. The MER is characterised by active oblique extensional tectonics, with a spreading rate of 6–7 mm/yr. It has an extension strain involving an increase in length of more than 5,000 km from the Red Sea up to Mozambique through the East African Rift System, where most of the great African lakes are located (Bonini et al., 2005).

As proposed by many authors (e.g. Bonini, 2005; Mohr, 1983; Woldegabriel et al., 1990; Hayward and Ebinger, 1996), the MER has been divided into three segments: (1) the Southern (2) the Central and (3) the Northern MER. These three segments symbolize distinct stages of the extensional processes, from early rifting in the Southern MER to the more gradually developed stages in the Central and Northern MER. The spreading has started to develop into normal seafloor spreading like the Afar (Hayward and Ebinger, 1996).

The main boundary faults in the southern, northern and central part of MER were formed around 18 Ma, about 10–11 Ma and around 8.3–9.7 Ma, respectively. Correspondingly, before the expected time syn-rift volcanism in the southern, northern and central MER was experienced in the area, in the beginning Miocene around 18–21 Ma, at about 10–11 Ma and about 8 Ma, respectively (e.g. Levitte et al., 1974; Zanettin et al., 1978; Woldegabriel et al., 1990; Ebinger et al., 1993; Kazmin et al., 1980; Mohr, 1983; Hayward and Ebinger, 1996; Chernet et al., 1998; George and Rogers, 2002; Wolfenden et al., 2004). The length of time from the start of faulting and volcanism inside the three rift segments points to a heterogeneous time-space evolution and forward movement of the continental rifting move in procession along the MER. The central MER will be discussed more below, as it is the sector which

includes the current study area. The central MER almost encircles the Lakes Region, up to the Lake Hawassa area, while the Addis Ababa - Nazret region is the transition zone between the central and the northern MER (Boccaletti et al., 1998). This part of the MER is characterised by the Yerer-Tullu-Wellel volcanic tectonic lineament (YTVL) to the north and the Goba–Bonga lineament (GBL) to the south (Figure 3).

Figure 5 shows the tectonic settings of the Main Ethiopian Rift. The transversal structures (YTVL to the north and GBL to the south of MER) were responsible for the discontinuation of the spread of rifting for a long period, therefore rifting in the MER did not proceed until about 8 Ma ago (Abebe et al., 2010). This is also determined by steep fault ridges such as the Munesa to the east and Guraghe rift margins to the west. These fault escarpments were the most significant development at the rift margins of the Central MER that took place about 3.5 Ma ago (e.g. Woldegabriel et al., 1990). They form a rounded line towards the rift and some authors regard them as the sources of felsic pyroclastic deposits and big caldera collapses (e.g. Woldegabriel et al., 1992). An important explanation for such conclusions is that the rounded escarpments of Munesa and Guraghe are associated with the more than 700 m thick
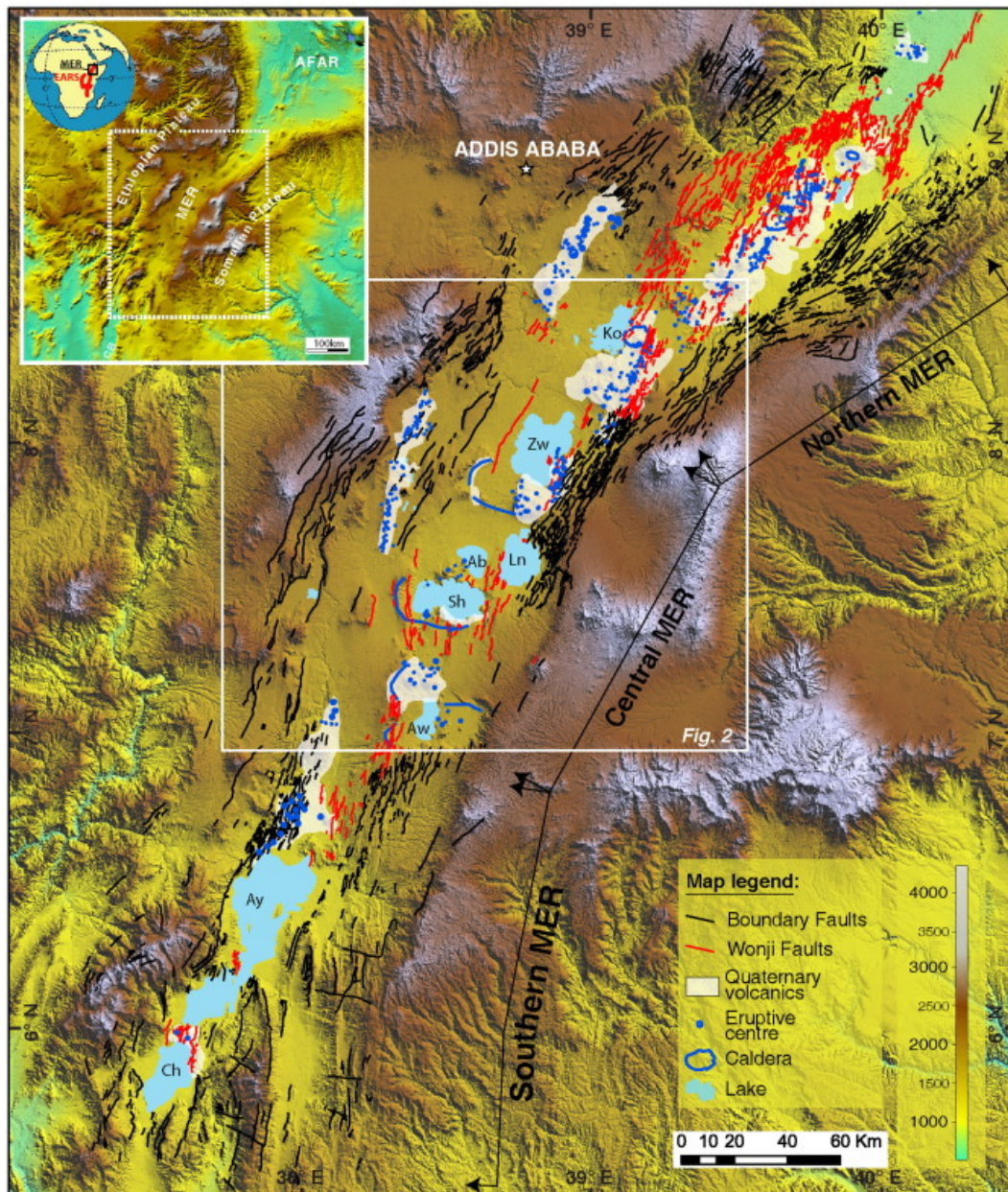
FIGURE 5: Tectonic setting of the Main Ethiopian Rift (MER) (Molin and Corti, 2015)

pyroclastic deposits that form basis in both escarpments. The MER is described by a set of NNE–SSW trending normal faults, the Wonji Fault Belt (WFB), and much of the active tectonic change in shape exists in the magmatic segments passing across these faults (Keir et al., 2006; Mohr, 1971). In the central MER, the edge faults are still seismically active (e.g. Hutchison et al., 2015) but in the south-western sector the main faults have decreased in activity and are gradually dying out. This is caused by the fact that the main faults are hidden by large quantities of volcanic products filling a possible former depression existing in the area. Active tectonic deformation that occurs in the magmatic segments of the central MER could be related to the geothermal system.

2.2 Previous exploration results from the Ashute, Butajira geothermal prospect

The geology of the Butajira area and Hosanna have been described through regional geological, geophysical and geochemical work which was conducted by various authors (Chernet et al., 1998; Woldegabriel et al., 1990). Abebe et al. (2017) reviewed previous geological studies of the Butajira area. In addition, a regional gravity survey was done with the objective of mapping high-density variations in the subsurface. This is considered valuable in facilitating new mineral discoveries, providing ground water targets for communities and attracting new investment.

3. OBJECTIVES OF THE STUDY

The main objectives of the geophysical studies are:

- To process MT data from the Ashute prospect and 1D invert the data. Present the resulting model as resistivity cross-sections and maps at different depths for geothermal interpretation;
- To pursue the resistivity anomaly mapped in Ashute in the general NE-SW direction and along the transverse faults in a different orientation and find the depth to the geothermal reservoir;
- To identify the subsurface resistivity distribution of the area, detect the characterization of a possible geothermal system and locate drilling targets.

3.1 Geothermal exploration

Geothermal exploration in Ethiopia has a long history. The estimated potential of geothermal resources in the country is more than 10,000 MWe. So far, only a small fraction of the total potential is harnessed. In order to avert possible shortfalls, and also due to their added advantage in complementing the hydro generation during unfavourable periods of severe droughts, geothermal development in Ethiopia has been given more attention in recent years (Kebede, 2014).

3.2 Geophysics - resistivity methods

Electromagnetic (EM) methods are inductive methods used to provide information on the conductivity structure of the subsurface. Inductive methods are most suitable in geothermal exploration. One of them is Magnetotellurics (MT) which is a passive geophysical method, using the natural magnetic field of the earth to investigate the electrical resistivity structure of the subsurface down to depths of several km (Vozoff, 1991). The transient electromagnetic method (TEM) is an active EM method. Here, an electric current is used to create a magnetic field in the Earth which is monitored as it decreases gradually when the source electric current is turned off. Together, the MT and TEM methods have been the most powerful tools in geophysical exploration for the last 2-3 decades and important in outlining the extent of geothermal resources.

3.3 Resistivity of rocks

Geothermal water interacts with rocks which undergo chemical and physical changes, including secondary mineralization, depending on the temperature and pressure. Resistivity depends on the type of mineral alteration, and the temperature and salinity of the fluid. The distribution of alteration minerals provides information on the temperature of the geothermal system, the flow path of geothermal water and the physicochemical characteristics of the geothermal water. At temperatures from about 100 to 220°C, low-temperature zeolites and smectite clay minerals are formed (Árnason et al., 2000). Smectite can be hydrated, and loosely bound cations between the silica plates make the mineral conductive with a high cation exchange capacity (CEC). Therefore, a conductive zone is formed where low-temperature zeolites and smectites are abundant. That zone is called the smectite-zeolite zone. In the temperature range from about 220 to about 250°C, the low-temperature zeolites disappear and the smectite changes to chlorite in a transition zone, called the mixed-layer clay zone, where smectite and chlorite coexist in a mixture. At about 250°C the smectite disappears and chlorite becomes the dominant alteration mineral. At even higher temperatures, above 250°C, epidote becomes abundant in the chlorite-epidote zone. This zoning is relevant for fresh water basaltic systems. The up-doming conductive smectite layer often indicates up flow of the system with corresponding outflows to its sides, away from the up flow.

Conforming to the usual standard, it was believed that the resistivity of a geothermal system decreases with increasing depth and increasing temperature. However, in high-temperature areas in a volcanic environment this is different. The conduction mechanism there is surface and pore fluid conduction. Figure 6 summarizes and explains the resistivity of the subsurface rock, alteration and temperature. The chlorite alteration zone indicates the existence of temperatures of 250°C or higher, assuming the alteration is in equilibrium with the temperature. If the geothermal system has cooled down, then the alteration remains the same and hence the resistivity structure as well. If this is the case, the interpretation
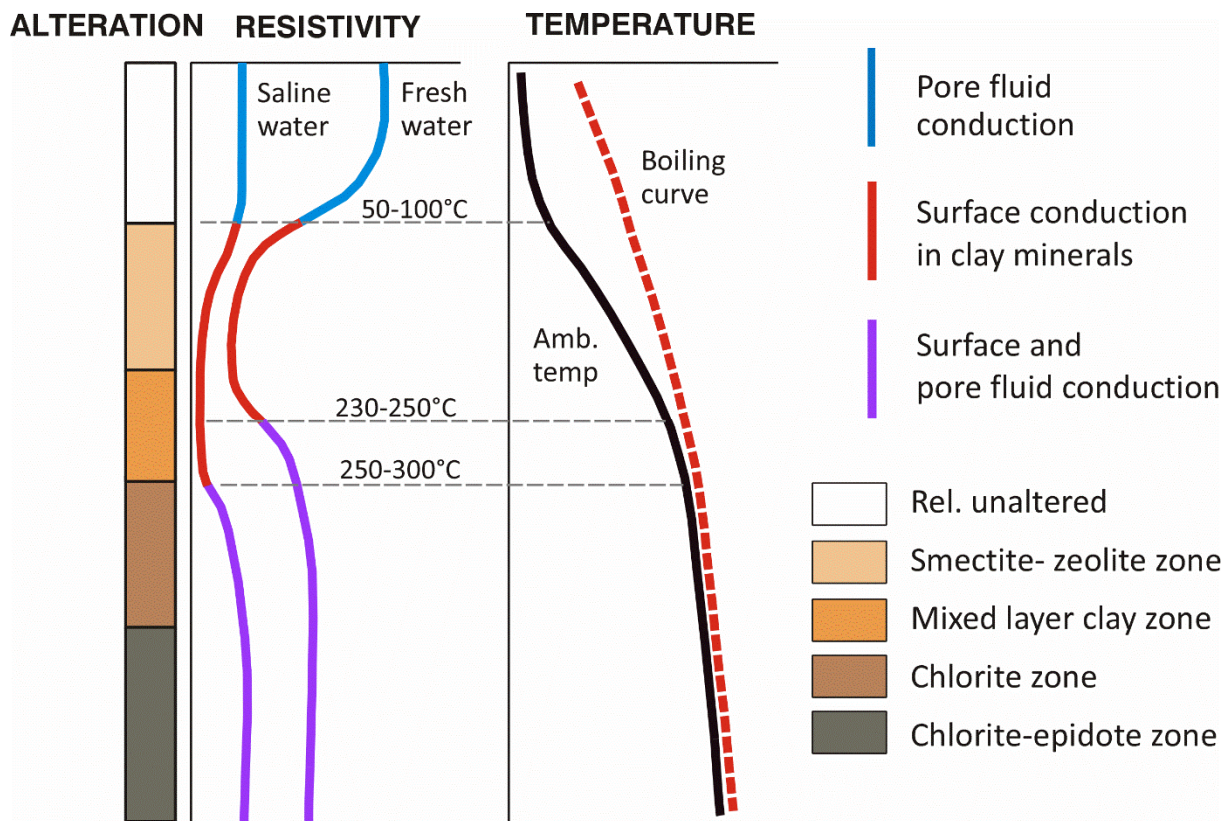
FIGURE 6: General resistivity structure of a high-temperature geothermal system in a volcanic environment showing resistivity variations with alteration and temperature (Flóvenz et al., 2012, modified from Flóvenz et al., 2005)

of the resistivity structure may be misleading since it shows alteration minerals that were formed in the past but not necessarily the current temperature. Alteration minerals can also show a sign of temperature which are lower than measured in the wells. This is interpreted as being due to a young system being heated up and the alteration is lagging behind, still not in equilibrium with the temperature (Hersir and Árnason, 2009).

4. THE MAGNETOTELLURIC METHOD

The MT measurements in this project were done with equipment from Phoenix. The method allows detection of resistivity anomalies associated with geothermal structures, including faults and the presence of a cap rock. This may allow an estimation of geothermal reservoir temperatures at various depths.

Different rocks, sediments and geological structures have a wide range of electrical conductivity. Measuring electrical resistivity allows distinguishing between different materials and structures and can improve knowledge of tectonic processes and geological structures. The Earth's naturally varying electrical and magnetic fields are measured over a wide range of frequencies, from 10,000 Hz to 0.0001 Hz (10,000 s). These fields are due to electrical currents in the Earth and the magnetic fields that induce them. The long periodic magnetic fields are produced mainly by the interaction between the solar wind and the magnetosphere. In addition, worldwide thunderstorm activity, mainly at equator causes magnetic fields at frequencies above 1 Hz. These natural phenomena create strong MT source signals over the entire frequency spectrum (Cagniard, 1953).

MT measurements can investigate resistivity at depths ranging from several hundreds of m to several km. Exploring great depths requires measuring low frequencies, which in turn requires long recording time. The horizontal resolution of MT mainly depends on the distance between sounding sites, the closer the soundings are, the greater is the horizontal resolution. Vertical resolution of MT mainly depends on the frequency measured, as lower frequencies have greater depth of penetration.

4.1 Electromagnetic theory

The MT method is an electromagnetic (EM) exploration method used to study the vertical and lateral subsurface resistivity distribution of the earth by measuring the electric and magnetic field components of the EM wave at the Earth's surface (Cagniard, 1953; Tikhonov, 1950). The theory and principle of the method are based on Faraday's and Ampere's EM induction laws described in Maxwell's equations.

In MT the naturally occurring electromagnetic (EM) field fluctuations that vary for a wide range of frequencies is measured. The source regions of the fields are the atmosphere/ionosphere and the magnetosphere. The low frequency signals range from a few Hz to periods of several thousands of seconds and are referred to as the MT frequency range, while the high frequency ranges from 1 Hz to more than 10^4 Hz, referred to as the AMT (Audio Magneto Telluric) signal and produced by thunderstorms close to the equator. EM fields in the MT range are used for deep investigation while EM fields in the AMT range are used for shallow investigation.

4.2 Depth of penetration of EM field – skin depth

At great distances from the source, the EM wave is a plane wave and when propagating the wave penetrates into the Earth, refracting downwards in the subsurface while the amplitude is attenuated at the same time. The depth of penetration of the wave in the Earth depends on the conductivity of the

subsurface and the frequency of the wave, and can be estimated through the skin depth given by the equation:

$$\delta \approx 500\sqrt{\rho/f} \text{ in m} \tag{1}$$

δ is known as the skin depth, the depth at which the amplitude of the wave is attenuated to 37% of its surface value, and f is the frequency of the EM wave.

From Equation 1 it can be seen for a given conductivity structure, that the penetration depth of the wave is proportional to the resistivity and inversely proportional to the frequency (Cagniard, 1953).

4.3 Propagation of EM waves in a homogeneous earth

In a homogeneous and isotropic medium, electromagnetic waves propagate in such a way that the electric and the magnetic fields are orthogonal to each other. The ratio of the electric field intensity to the magnetic field intensity, $E_x(\omega)/H_y(\omega)$, is known as the impedance tensor element Z_{xy} (see, e.g. Cagniard, 1953; Keller and Frischknecht, 1966). It is a measure of the electromagnetic property or the response of the earth and is given by:

$$Z_{xy}(\omega) = E_x(\omega)/H_y(\omega) = i\omega\mu/\kappa, \text{ where: } \kappa = \sqrt{i\omega\mu(\sigma + i\omega\epsilon)} \approx \sqrt{i\omega\mu\sigma} \tag{2}$$

κ is the propagation constant of the medium, ϵ and μ are the dielectric permittivity and magnetic permeability of the medium, respectively, and ω the angular frequency of the wave.

From the relationship above, for a homogeneous and isotropic medium the true resistivity, ρ is calculated through:

$$\rho_{xy} = 1/\sigma = 1/\omega\mu \left| Z \right|^2 = 0.2 \ T \cdot \left| E_x/H_y \right|^2 \text{ and the phase } \varphi = arg(Z) = 45° \tag{3}$$

where T is the period of the wave.

Since our medium is homogeneous and isotropic, the resistivity ρ is the same for all ω and the result is the same in all directions. Hence, $\rho_{xy} = \rho_{yx} = \rho$ and the phase between the electric and magnetic field, φ is 45°. However, Z_{xy} and Z_{yx} have opposite signs (Vozoff, 1991).

In the case of a non-homogenous earth, the resistivity, ρ and phase, φ depend on the frequency ω. Hence, instead of the true resistivity and phase, the definition of apparent resistivity $\rho_a(\omega)$ and phase $\varphi_a(\omega)$ are introduced:

$$\rho_a(\omega) = 1/\omega\mu \left| E_x(\omega)/H_y(\omega) \right|^2 = 0.2 \ T \left| E_x(\omega)/H_y(\omega) \right|^2, \text{ and the phase } \varphi_a(\omega) = arg(Z_0) \neq 45° \tag{4}$$

where Z_0 is the impedance at the surface.

5. MAGNETOTELLURIC RESPONSE FUNCTIONS

The relationship between the measured EM field components $(E_x, E_y, H_x, H_y, H_z)$ at a single site is contained in the impedance tensor and the Tipper (Vozoff, 1972). The Tipper is also known as MT transfer functions or MT response functions. These parameters are useful in the interpretation of subsurface resistivity distribution around the measurement the site.

5.1 Impedance tensor

In general, the apparent resistivity for each frequency varies with respect to the orientation of the measurement setup. The electric field E_x is partly induced by H_y, but also partly produced by currents

induced by H_x, which have been affected by the underground resistivity structure. The same is true for the electric field E_y. For the generalized situation, the measured EM field components at each frequency behave as a linear system expressed through the following relations:

$$E_x = Z_{xy}H_y + Z_{xx}H_x$$
$$E_y = Z_{yx}H_x + Z_{yy}H_y \tag{5}$$

In matrix form this is commonly written as proposed by Cantwell (1960) and Vozoff (1972):

$$\begin{pmatrix} E_x \\ E_y \end{pmatrix} = \begin{pmatrix} Z_{xx} & Z_{xy} \\ Z_{yx} & Z_{yy} \end{pmatrix} \begin{pmatrix} H_x \\ H_y \end{pmatrix}, \boldsymbol{E = ZH} \tag{6}$$

Z_{xx} and Z_{yy} are referred to as diagonal elements of the impedance tensor and Z_{xy} and Z_{yx} as off diagonal elements or principal impedances. The impedance tensor elements can be evaluated for different cases as follows:

Case 1: For a 1D earth, uniform or horizontally layered earth, conductivity varies only with depth. Hence, the MT impedances are independent of the orientation of the measurement axes:

$$Z_{xx} = Z_{yy} = 0 \text{ and } Z_{xy} = -Z_{yx}$$

and the apparent resistivity and phase obey Equation 3.

Case 2: For a 2D Earth, where one of the measurement's axis is aligned along the geo-electric strike direction: the resistivity is constant in this direction and varies in the other horizontal perpendicular direction and with depth. If the x axis is set parallel to the strike then:

$$Z_{xx} = Z_{yy} = 0 \text{ and } Z_{xy} \neq -Z_{yx}$$

In this case Maxwell's equations decouple into two modes, *TE* mode, referred to as transverse electric or E-polarization, and *TM* mode or transverse magnetic or *B*-polarization. This may be expressed as:

$$Z_{xy} = TE \text{ and } Z_{yx} = TM \tag{7}$$

Case 3: For a 3D earth, all impedance tensor elements are different and no geo-electric strike exists.

5.2 Geomagnetic transfer functions

The geomagnetic transfer function, Tipper vector or Tipper (T), is a complex vector that relates the vertical and the two horizontal components of the magnetic field and is imbedded in the relation:

$$H_z(\omega) = T_x H_x(\omega) + T_y H_y(\omega) \tag{8}$$

T_x and T_y are the *x* and *y* components of the Tipper, respectively. The Tipper is a dimensionless complex vector including phase. $H_z(\omega)$ is induced in the vicinity of vertical boundaries of conductivity contrasts. In the case of a homogeneous or 1D Earth, no $H_z(\omega)$ is induced, and hence T_x and T_y are zero. The Tipper vector can be decomposed into two real vectors in the horizontal *xy*-plane, known as induction arrows. The arrows are used to infer the presence of inhomogeneity or lateral conductivity variations and also to resolve ambiguity in dimensionality. Two representations of the induction arrows are known; Parkinson convention (Parkinson, 1959) and the reversed one (Schmucker or Wiese convention). In the Wiese convention the real part of the induction arrows point away from conductive zones (Wiese, 1962) and can be used to determine the geo-electric strike direction of the area.

6. INSTRUMENTATION, DATA ACQUISITION AND PROCESSING

6.1 Instrumentation and data acquisition

The MT survey in Butajira, Ashute field was conducted on eight profiles. They stretch over the area of geothermal surface manifestations and are oriented nearly perpendicular to the general regional structural trend, the NE-SW direction (Figure 7). The profile and station intervals are about 1 and 1.5 km, respectively, while in Ashute the profiles are laid out as infill profiles close to the surface manifestations (Table 2).
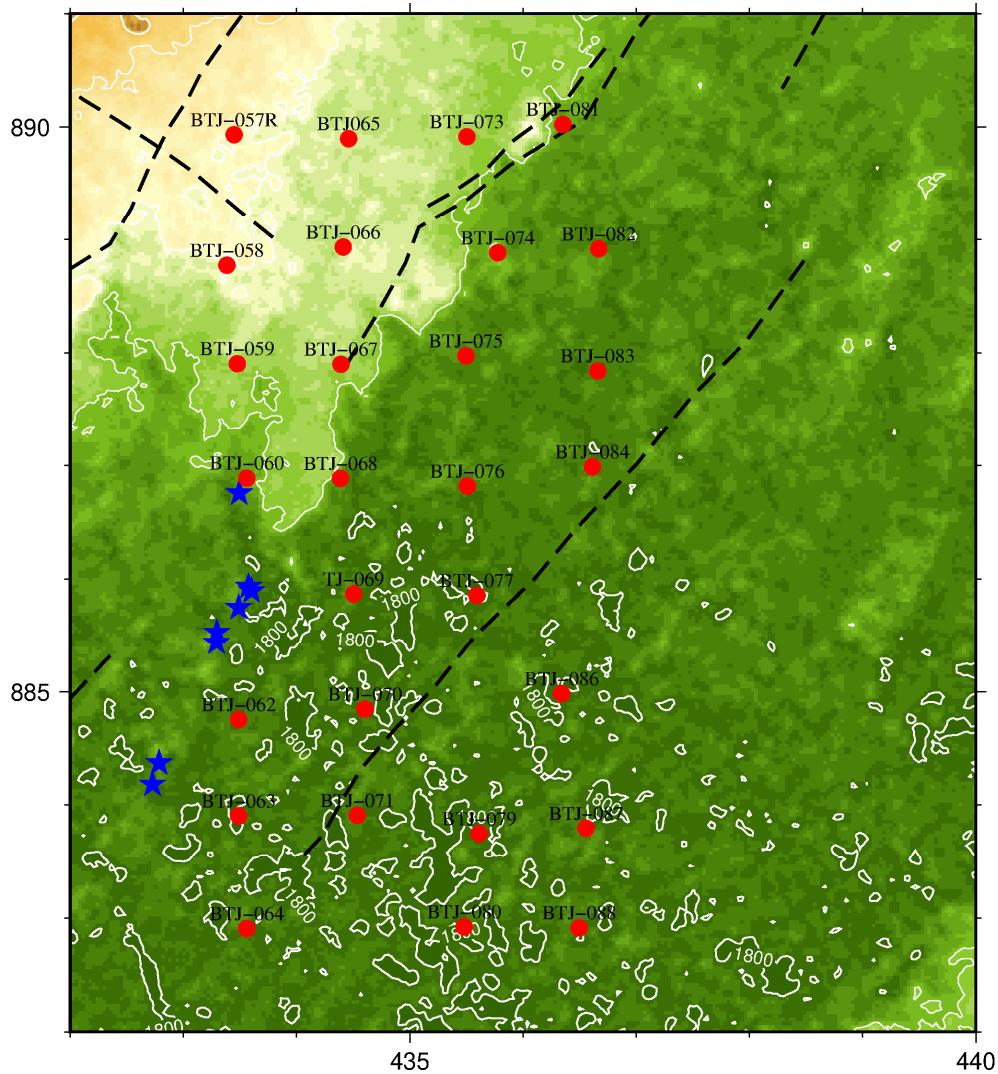
FIGURE 7: Location of the MT stations (red dots); blue stars are geothermal surface
manifestations and the black dashed lines are faults

TABLE 2: Summary of the MT work

Geophysical method	Data type	Measurement distribution pattern	Profile interval (km)	Sounding interval (km)	Number of soundings
Magnetotelluric (MT)	Single reading at a single sounding	Parallel profiles	1-1.5	1	28
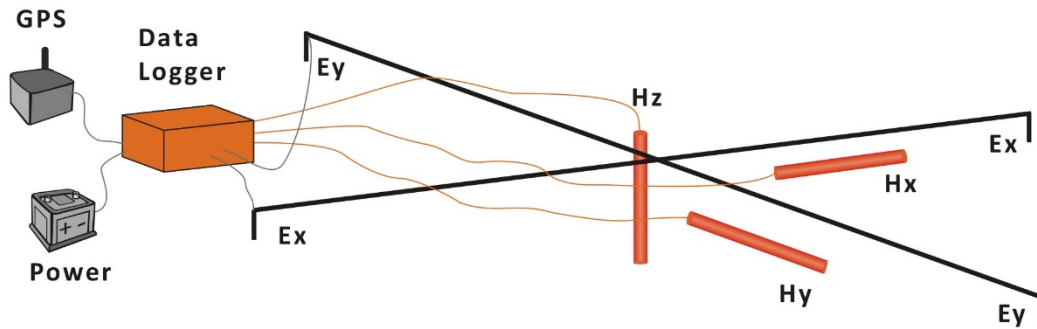
FIGURE 8: MT field survey layout (Flóvenz et al., 2012)

In this study, MT data were acquired by setting the electric field and magnetic field sensors orthogonal to each other and setting the x-axis in the geographic north direction as shown in (Figure 8).

On each survey day, two MT measurements were done and the time series of the amplitudes of the five components of the EM field (E_x, E_y, H_x, H_y and H_z) were recorded by the data logger at the centre. The time series data were recorded for about 21 hours between 10 AM and 7 AM. The electromagnetic fields were in the frequency range between 320 and 0.001 Hz. From this frequency range, MT parameters at more than 50 frequencies were calculated.

In the survey, two sets of MT equipment from Phoenix were used. The two sets include MTU5-A data loggers with serial numbers 2172 and 4013, magnetic induction coils MTC-50, lead chloride porous pots as electric field sensors, dipole cables and magnetic coils. Navigations to the preloaded stations were made using a handheld Garmin GPS. During the field setup a compass was used to align the electric and magnetic field sensor lines. The magnetic induction coils were levelled, and buried in small trenches and covered with dirt to avoid mechanical shock and direct sun light. The recorded time series data were stored in a 540 MB compact flash card in the data logger and retrieved to a computer for later processing.
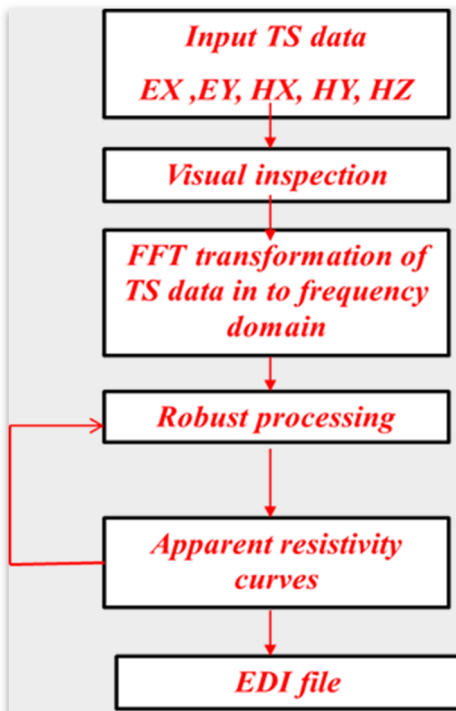
FIGURE 9: Data processing and interpretation flow chart (Phoenix Geophysics, 2005)

6.2 Data quality evaluation and processing of time series

Data processing and interpretation generally involve two stages as indicated on Figure 9. The processing steps in the flow chart were mostly carried out using the software SSMT2000, Synchro time series viewer and MTEditor from Phoenix Geophysics (2005).

Data processing involves various actions. First the data from the compact flash are downloaded onto a laptop computer. Visual inspection of the recorded data on site and a preliminary time series processing in the field camp were done on a daily basis to ensure acceptable data quality for later processing and interpretation. This is followed by transformation of the time series data from time domain to the frequency domain.

The robust processing is a multiple coherency based stacking of spectra, a routine statistical method derives estimates of the MT impedance tensor elements. MT response functions that are relatively smooth unbiased by outliers, were done in SSMT2000. With reference to these parameters on the

display, cross-power data consisting of 40 segments were edited to reduce noise and standard deviation, and enhance resistivity continuity to ensure data quality (Phoenix Geophysics, 2005).

6.3 1D inversion of MT data using the TEMTD Program

The TEMTD program can perform 1D inversion for both TEM and MT data, separately or jointly (Árnason, 2006). TEMTD solves both the forward and inverse problems. The inversion problem is to find those model parameters which give a model response close to the measured data. The forward problem calculates the response from given model parameters. The programme gives the possibility of keeping the model smooth with respect to resistivity variations between layers.

7. RESULTS OF MT RESISTIVITY MODELLING FROM ASHUTE GEOTHERMAL FIELD

Interpretation of the MT data is the second stage in the data processing and interpretation sequence (Figure 10). First, it is necessary to check the static shift of the data. Then the data are analysed and inverted to yield an electrical resistivity structure of the earth below the measurement site and its variation, both laterally and vertically. The directionality and dimensionality of the impedance tensor and its changes with frequency (depth) are evaluated and determined. The processed data from all the MT soundings are found in Appendix I in the Appendices report (Tadesse, 2018).
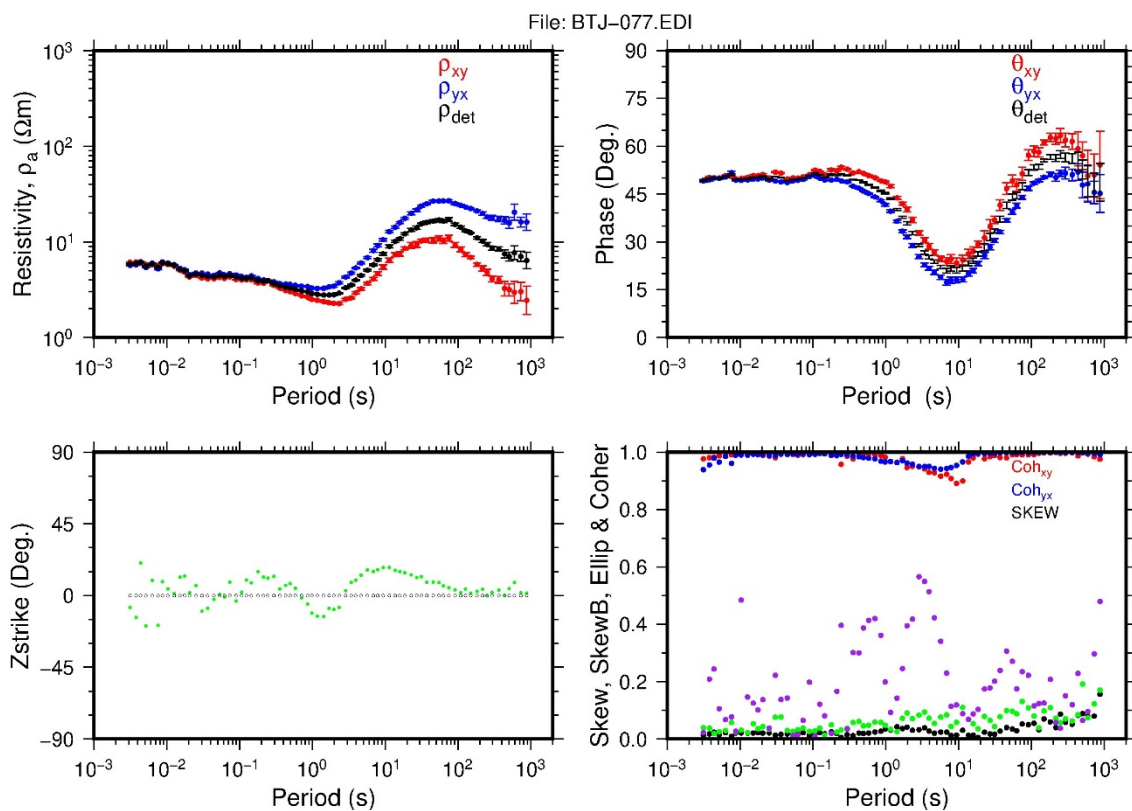
FIGURE 10: An example of processed MT data (station BTJ-077) from the prospect area; The apparent resistivity and phase for the different parameters: ρ_{xy} and ρ_{yx}, and ρ_{det}, which is derived from the determinant of the impedance tensor, are shown on the figure as well as the Z-strike, skew, ellipticity and coherency

A 1D inversion is performed and the resistivity model integrated with other geoscientific data. In this project area, 1D resistivity models were obtained as well as maps and cross-sections produced in Linux.

Data from the EDI files for each MT station, output from MTEditor, were inverted using the TEMTD program (Árnason, 2006). Occam inversion was used and the input was the rotationally invariant apparent resistivity and phase calculated from the determinant of the impedance tensor (see e.g. Lemma, 2010). The project covered inversion of MT data from 28 stations (location is shown on Figure 7).

7.1 1D inversion of MT data from Ashute

The apparent resistivity and phase were inverted assuming a smoothed 1D earth model. The resistivity varies only with depth and hence, the MT impedance tensor is independent of the orientation of the measurement axes. Target zones are areas of relatively low resistivity that could be associated with conductive pyroclastic ash flow deposits, sediments and hydrothermally altered zones, showing significant areal distribution and thickness within a relatively shallow depth range. These might be underlain by zones of relatively high resistivity that could be correlated with high-temperature alteration zones that would possibly indicate the core of a high-temperature geothermal reservoir. Resistivity discontinuities might serve as structures for the circulation of geothermal fluid.

Figure 11 shows an example of 1D Occam inversion of MT data. All the inversion models are presented in Appendix II in the Appendices report (Tadesse, 2018).
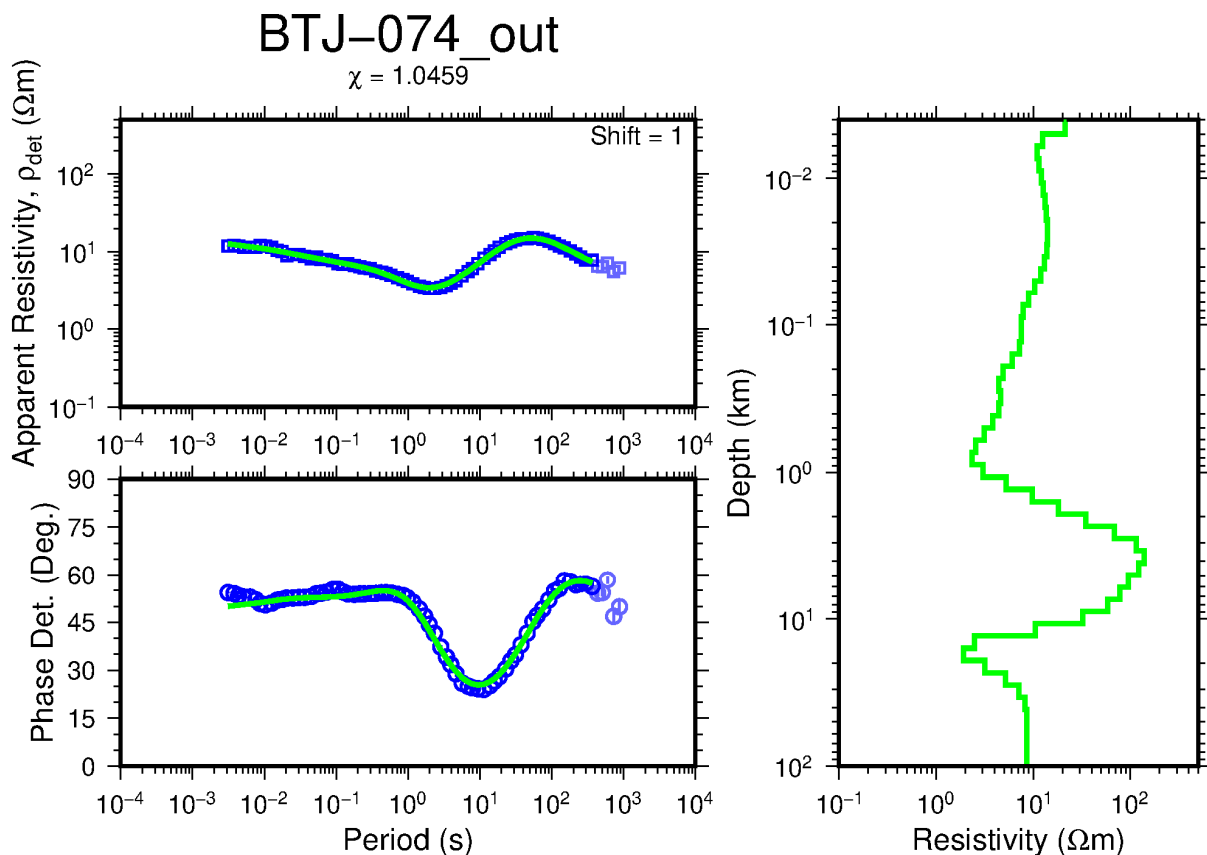
FIGURE 11: 1D Occam inversion of MT sounding BTJ-074, as seen at the top of the Figure, while χ is the misfit. Blue squares are the apparent resistivity and blue circles the phase, both calculated from the determinant value of the impedance tensor. The light blue symbols to the right of the green curve are data points not used in the inversion, the green curves on the panels to the left show the MT apparent resistivity and phase responses from the resistivity model to the right

The 1D models provide information on the resistivity structure of the subsurface versus depth. The models are often presented as resistivity cross-sections and depth maps. Zones of low-resistivity values at shallow depths are often the cap rock of the geothermal reservoir. The underlying relatively higher resistivity zone, the resistive core, is often associated with high-temperature hydrothermal alteration zone while resistivity discontinuities might serve as conduits for the circulation of geothermal fluid.

The conductive zone in Ashute delineates a zone marked by 10 Ωm or less. It is observed to have a general NE-SW orientation that extends from the surface to a maximum depth of about 450 m. The zone is flanked to the northeast and southwest by slightly higher resistivity. In the southwestern portion, the Ashute hot springs and hydrothermally altered zone coincide with a slightly higher resistivity zone.

In general, the marginal Debre zait Selti rift graben suggests a main NE – SW Debre zait Selti fault system and a transverse NW – SE older rift structure control the magmatism (heat source), water recharge and the permeability of the system. Two possible heat sources are expected, which are directly associated with the young basaltic eruptions and intrusions younger than 0.13 Ma and silicic centers located in the southern part of the area. Possible enrichment of these units by shallow/deep geothermal fluid is expected to enhance the conductivity as can be witnessed from very low resistivity values observed on these maps.

The influence of the NE-SW and NNE structures are more evident in the low resistivity contours at Ashute on most of the maps. That might reflect its association with high permeability around the intersection of faults/fractures with varying orientations. A trace of an ENE structure could be inferred in the Ashute area and the observed central low resistivity contours seen on most of the maps are still opened towards the south east.

7.2 The resistivity cross-sections from Ashute

Resistivity cross-sections were produced using the TEMCROSS programme developed at ISOR (Eysteinsson, 1998) along eight resistivity profiles based on the 1D resistivity models shown in Appendix II in the Appendices report (Tadesse, 2018). The location of the soundings is shown on Figure 7. Resistivity cross-sections along profile 1 and profile 3 are discussed below. The eight cross-sections are given in Appendix III in the Appendices report (Tadesse, 2018).

Resistivity cross-section along profile 1 is shown in Figure 12 down to a depth of 5,000 m b.s.l. and on Figure 13 down to a depth of 1,000 m b.s.l. Similarly, the cross-section along profile 3 is shown on Figure 14 down to a depth of 5,000 m b.s.l. and in Figure 15 down to a depth of 1,000 m b.s.l. The cross-sections generally display three resistivity layers in the Ashute field. The first layer is marked by low-resistivity values, less than 10 Ωm. It is observed to stretch across the two profiles with varying thicknesses. On profile 3, east of MT sounding BTJ-067, the layer is 1,400 m thick and reaches down to a depth of 400 m a.s.l. Both cross-sections are fairly similar and the prospect area is flat. The subsurface is composed of volcanic sediments including lithified ash, fine- to coarse-grained sandstone, well laminated conglomerate and debris or lahar. The clasts mostly consist of pyroclastic material derived from a silicic centre from the south. They can be correlated with sediments at shallow depth and a low resistivity of less than 10 Ωm.

The resistivity cross-section along profile 1 indicates a fault trending NE-SW parallel to the general geological structures. From 1,600 m a.s.l. down to sea level, a layer of very low resistivity, less than 10 Ωm, is displayed on the cross-section, probably consisting of sediments and sandstone. At a depth of 2,000-5,000 m b.s.l. basaltic and probably high-temperature alteration minerals deposits are found as the resistivity increases to more than 100 Ωm.

The shallow lying conductive layer in the cross-section along profile 3 indicates a structure between station BTJ-059 and BTJ-067. The low-resistivity layer on the cross-section, is nearly uniform in
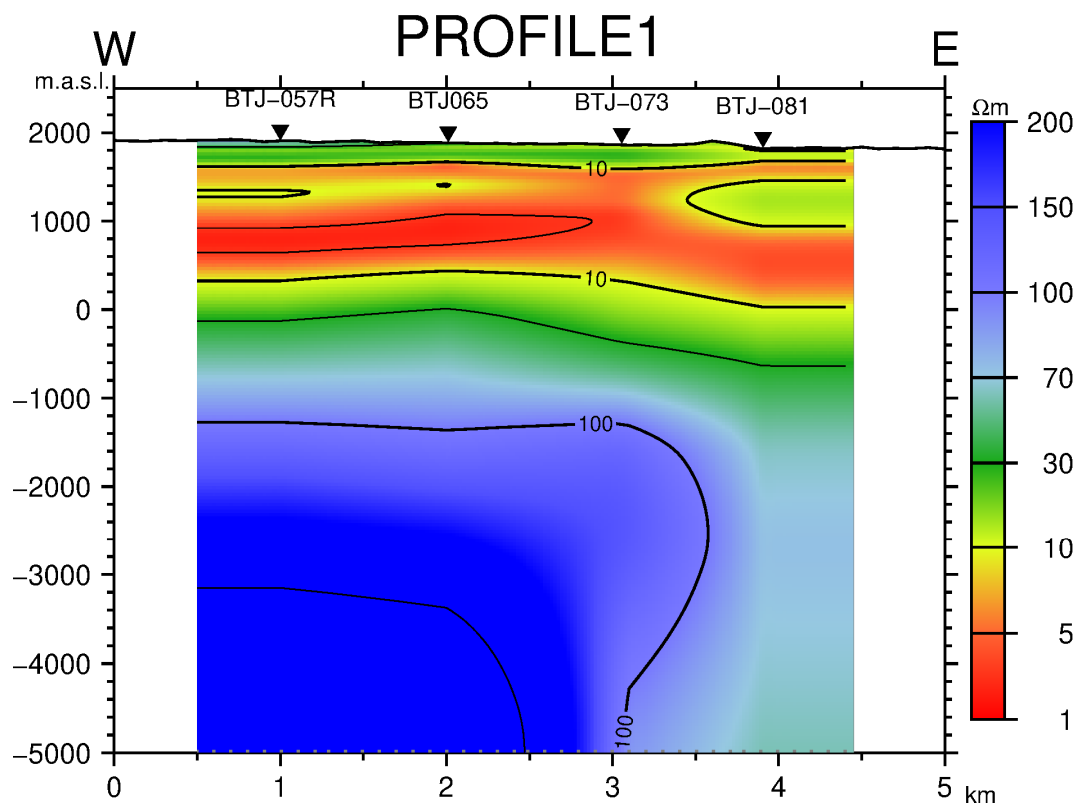
FIGURE 12: Resistivity cross-section along profile 1 down to a
depth of 5,000 m b.s.l.; location is shown in Figure 7
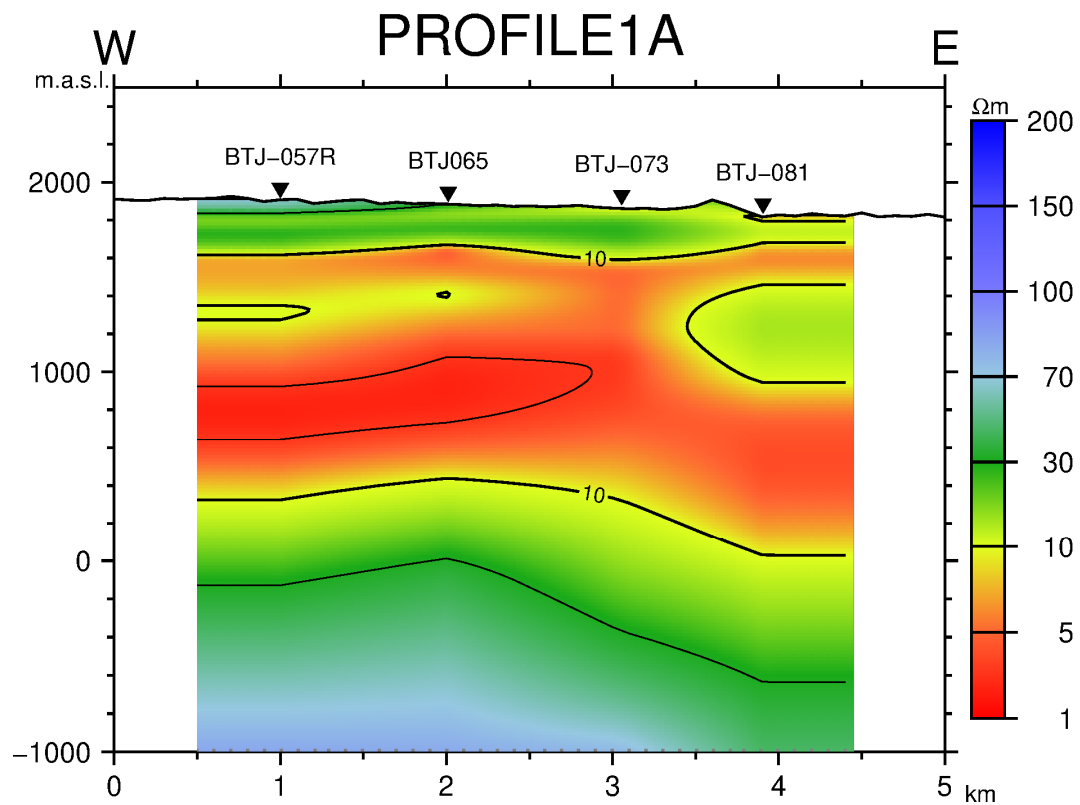
FIGURE 13: Resistivity cross-section along profile 1 down to a
depth of 1,000 m b.s.l.; location is shown in Figure 7
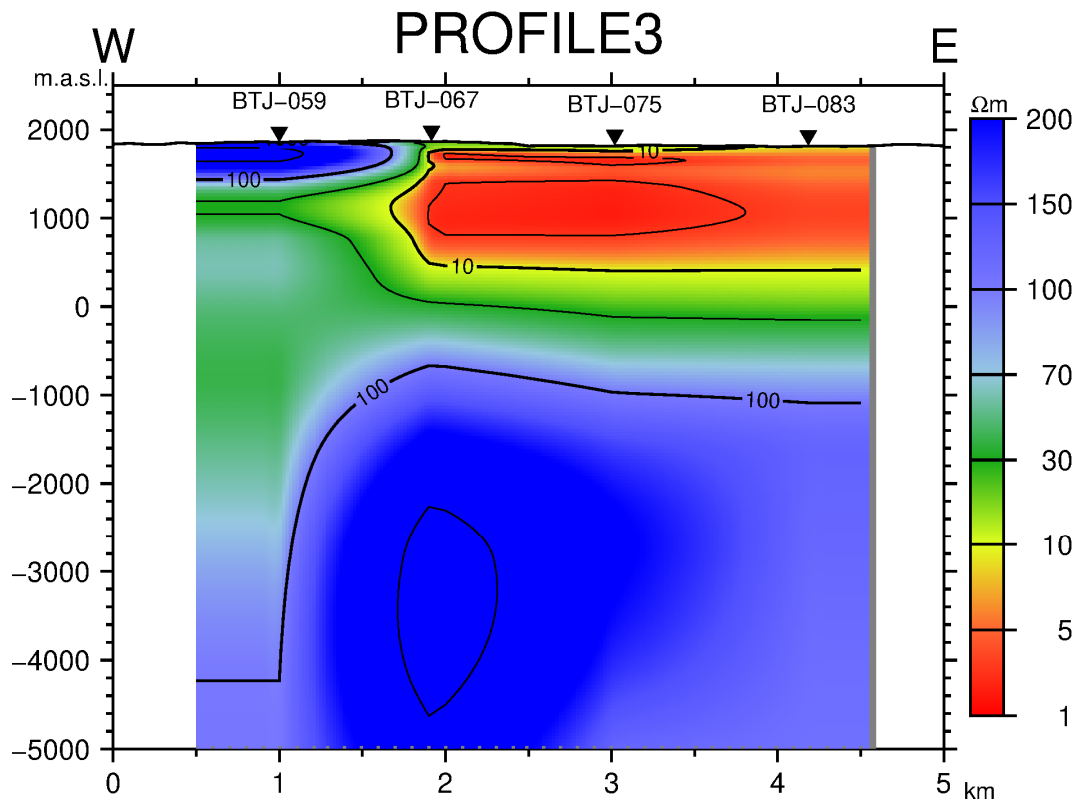
FIGURE 14: Resistivity cross-section along profile 3, down to a
depth of 5,000 m b.s.l.; location is shown in Figure 7
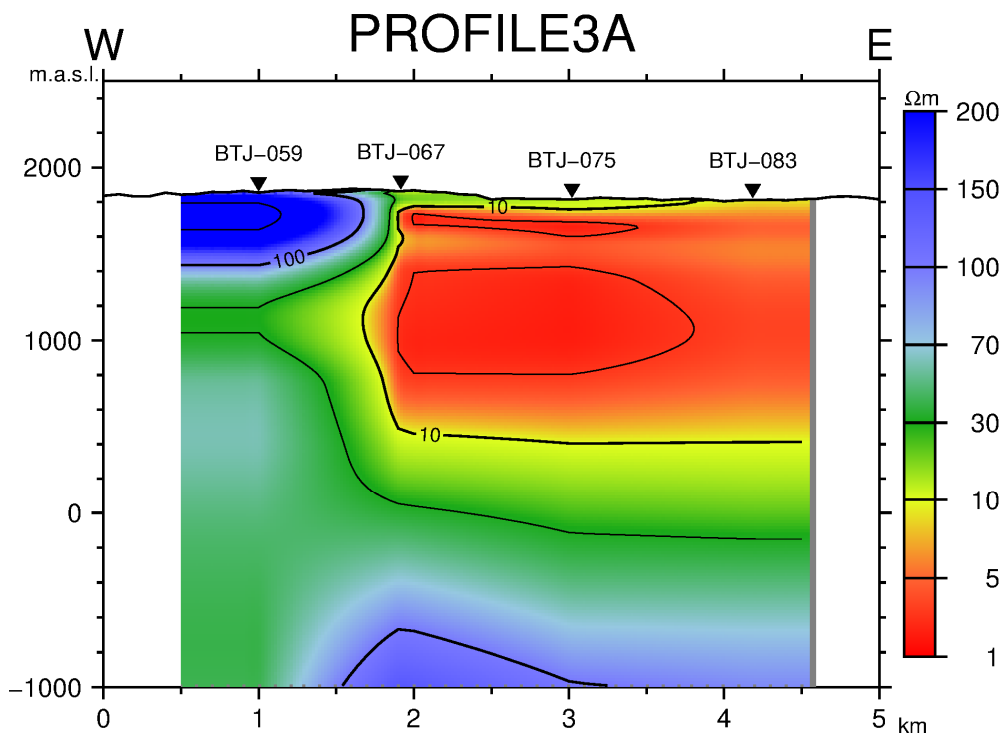
FIGURE 15: Resistivity cross-section along profile 3, down to a
depth of 1,000 m b.s.l.; location is shown in Figure 7

thickness, around 1,400 m reaching down to a depth of 400 m above sea level. This layer is not seen below station BTJ-059.

All the resistivity layers extend in general across the whole profiles with the exception of MT station BTJ-059 where the vertical resistivity boundaries observed, are associated with the second layer. High resistivity below the conductive layer is seen across most of the profiles.

7.3 Resistivity maps from Ashute

Resistivity maps were produced using the TEMRESD programme developed at ISOR (Eysteinsson, 1998) to plot horizontal resistivity maps based on the 1D layered resistivity models as shown in Appendix II in the Appendices report (Tadesse, 2018). Two depth maps are discussed below, at 1,000 m a.s.l. (Figure 16) and 500 m b.s.l. (Figure 17). All the calculated depth maps are given in Appendix IV in the Appendices report (Tadesse, 2018).

Resistivity map at 1,000 m a.s.l. (Figure 16): In general, the map displays very low resistivity, between 1 and 5 Ωm, in the north and northeast part of the survey area. A fairly high resistivity, around 70 Ωm, is observed in the southwest part of the area. The discontinuity in the Debre zait Selti graben suggests that the main NE-SW fault system associated with Debre zait Selti, and the transverse NW-SE older rift structure control the magmatism (heat source), water recharge and permeability of the system. The overall low resistivity in the area is an attribute of the thick lacustrine sediment deposits intercalated with pyroclastic ash flow in the Ashute field. The high resistivity seen on the maps at shallow levels around Ashute signifies the recent and sub-recent basalt flows, phreatomagmatic deposits and volcanic crater lake in which basalt is intensively weathered from bottom to top of the crater. The high resistivity mapped around Ashute could be a response to the recent and sub recent basalt flow.
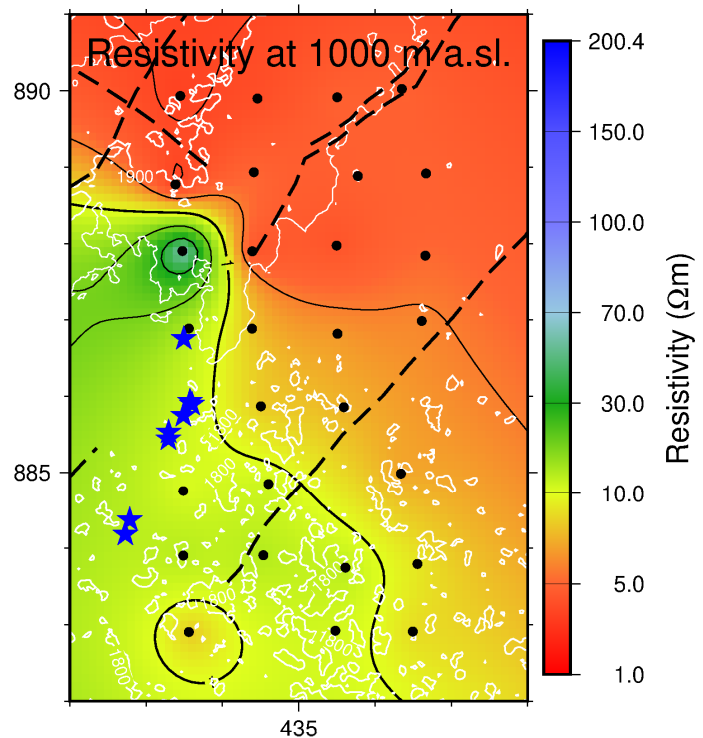
FIGURE 16: A map showing resistivity in the Ashute prospect area at 1,000 m a.s.l. The blue stars are geothermal surface manifestations, the black dashed lines are faults, and black dots are MT soundings
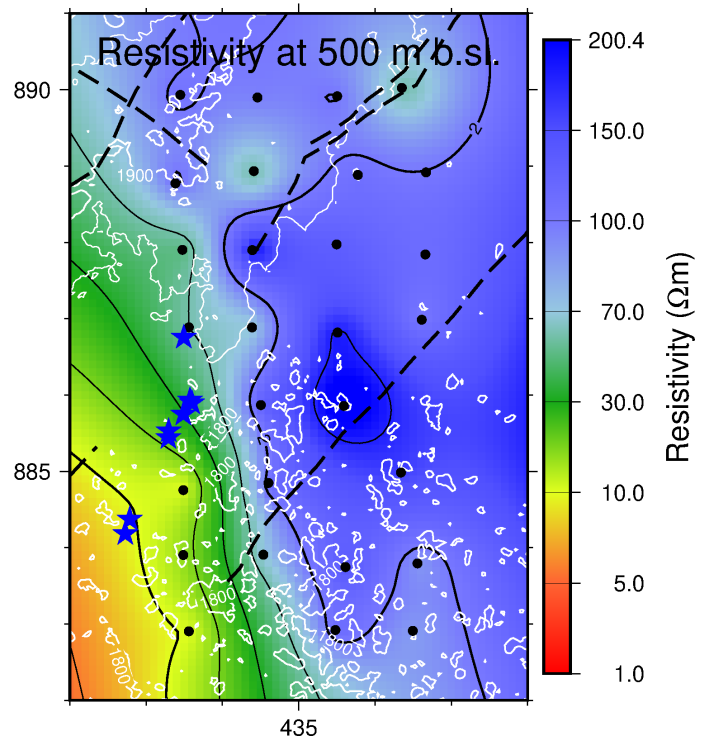
FIGURE 17: A map showing resistivity in the Ashute prospect area at 500 m b.s.l., for figure legend see Figure 16

Resistivity map at 500 m b.s.l. (Figure 17): The high resistivity in the northeast part of the survey area, greater than 70 Ωm, is probably because of lithological variations due to recent and sub recent basalt flow and phreatomagmatic deposits. The resistivity structure is oblique to the old NW-SE rift structure.

8. STRIKE ANALYSIS

Z-strike is determined through a horizontal rotation that maximizes the off-diagonal elements of the MT impedance tensor and minimizes the diagonal elements using the sum of the squared modulus of the elements. The Z-strike has 90º ambiguity and the strike direction can't be determined from the MT impedance alone. This ambiguity is resolved using a parameter that doesn't depend on the impedance tensor elements, known as Tipper vector, provided that H_z is measured at the measurement site (Vozoff, 1991). The generalization of dimensionality is also made using the Tipper magnitude of the magnetotelluric transfer function. The magnitude of the Tipper depends on the presence of lateral conductivity variations. Low Tipper magnitude, very close to zero, is related to 1D resistivity structures while high Tipper magnitude implies, generally, non-1D conductivity structure.

Strike analyses have been performed in this work by producing maps showing induction arrows at 10 s (Figure 18), a rose diagram of the Tipper strike for 0.5-1 s (Figure 19) and a rose diagram of the Z-strike for 0.1-0.5 s (Figure 20). These maps are discussed below. Additional maps showing results from the strike analyses are presented in Appendix V in the Appendices report (Tadesse, 2018).

Figure 18 shows the induction arrows at a low frequency (0.1 Hz) or great depths. The arrows are small, indicating small resistivity contrasts at these depths as seen on the resistivity maps above. The Tipper strike in Figure 19 is shown for low frequency (1-2 Hz), reflecting relatively great depth while Figure 20 shows the geoelectrical strike direction at shallow depths (high frequency; 2-10 Hz) reflecting the dominant NE-SW geological strike direction of the area. Note, however, the change of the strike direction in the northwest corner of Figure 20.

Induction arrows at 10 s
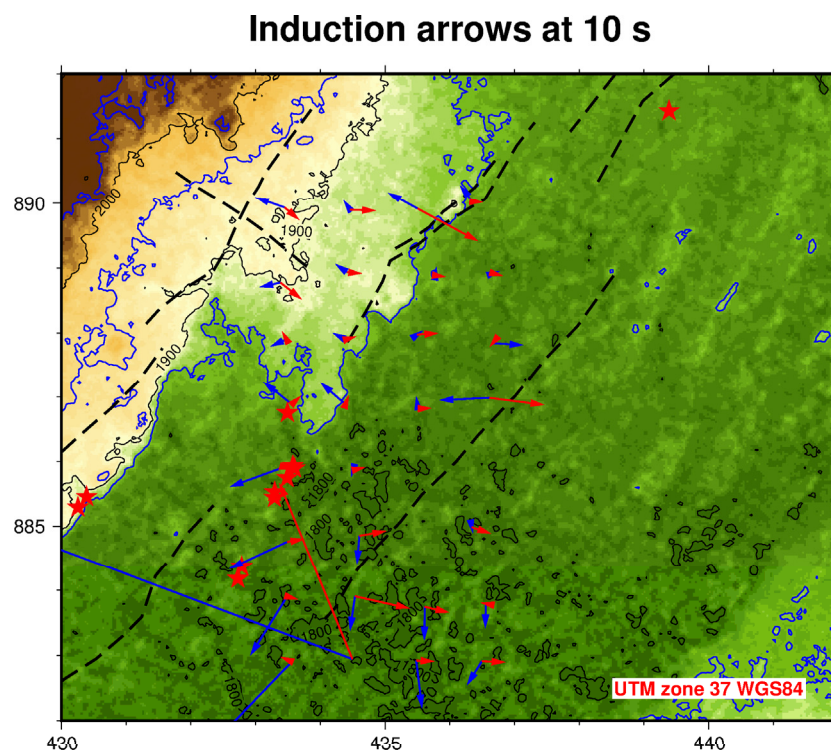
FIGURE 18: Induction arrows at 10 s; red arrows are the imaginary part and blue arrows the real part; red stars are geothermal surface manifestations and the black dashed lines are the faults

T–strike at 0.5–1 s
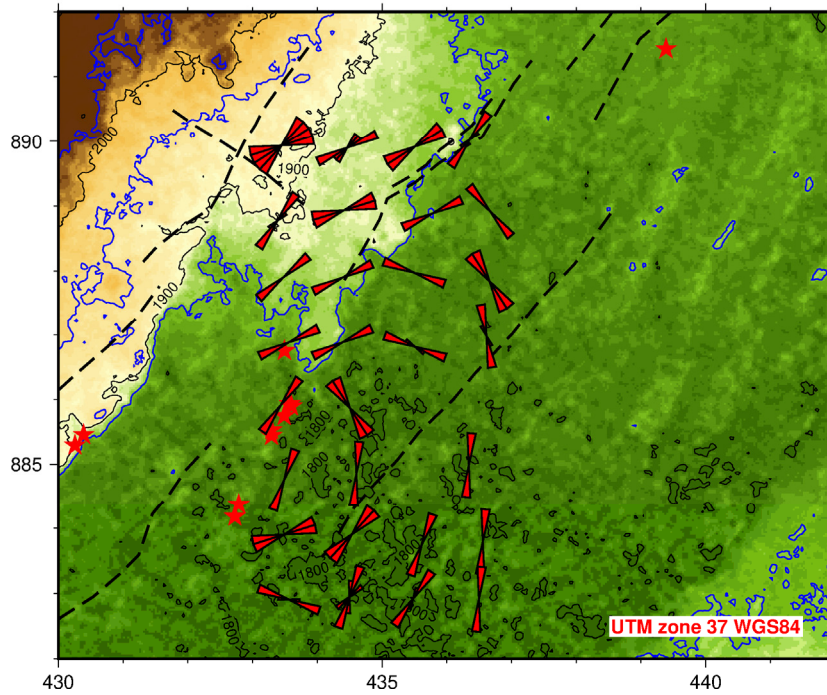
FIGURE 19: Rose diagram showing the Tipper strike at 0.5-1 s;
red stars are geothermal surface manifestations and the black dashed lines are the faults

Z–strike at 0.1–0.5 s
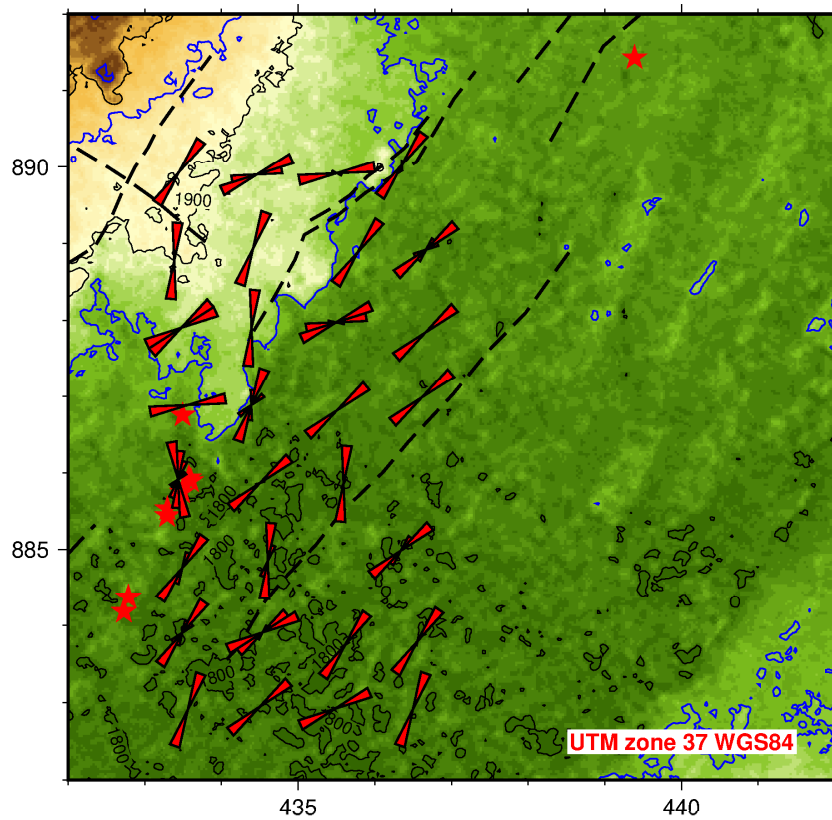
FIGURE 20: Rose diagram showing the Zstrike at 0.1-0.5 s;
red stars are geothermal surface manifestations and the black dashed lines are the faults

9. CONCLUSION

In this project 28 MT soundings have been processed and 1D inverted. The results are presented as resistivity cross-sections and maps and compared to the geological findings. The sporadic nature of the orientation of the resistivity contour lines for different depth levels suggests that the Ashute field is structurally complex, as indicated by the presence of the different orientations of the faults and fractures in the area.

The Ashute area is characterized by a shallow lying conductive layer with resistivity values less than 10 Ωm and an average thickness of about 1,600 m in general. It reaches down to a depth of 200 m a.s.l. The subsurface is composed of volcanic sediments including lithified ash, fine- to coarse grained sandstone, well laminated conglomerate and debris or lahar. The clasts consist mostly of pyroclastic material derived from a silicic centre in the south. They can be correlated with sediments at shallow depth and low resistivity. Below the low resistivity, high resistivity is found, greater than 70 Ωm, which is probably related to the basement, fractured basalt and scoria. This high resistivity reflects likely the influence of major fault systems, the tectonic trend of the Debre zait Selti rift graben and the Main Ethiopian Rift (MER).

Most likely, geothermal fluid at depth emerges to a shallow level along the NE-SW discontinuity and NW-SE structures, flowing laterally and enriching the shallow permeable formation, and appearing as thermal manifestations in the field.

The strike analyses for different frequencies (depth levels) indicate a general NE-SW strike direction at shallow depths which coincides with the major trend of the western rift axis. At greater depths the geo-electrical structure changes.

10. RECOMMENDATIONS

No TEM soundings were carried out as a part of this project. Therefore, it is recommended to do TEM at the same locations as the MT sites to correct for the static shift of the MT data. Furthermore, to jointly invert the TEM and MT data. This should be carried out before any decisions are made on drilling in the study area. It is furthermore recommended to add data towards the north and west of the Ashute field, including both MT and co-located TEM soundings, to better define the resistivity structures. Detailed geological mapping of the area, in particular with regards to tectonics is recommended, and also gravity surveying to delineate geological structures.

Finally, I would like to acknowledge with gratitude and thanks for the support and love of my family. Also, thank you all 6-month UNU Fellows and colleagues, especially my geophysical colleagues.

REFERENCES

Abebe, T., and Alemu, T., 2007: Geology and tectonic evaluations of the Pan-African Tulu Dimtu Belt, Western Ethiopia. *J. Earth Sciences, 1-1,* 24-42.

Abebe, T, Balestrieri, M.L., and Bigazzi G., 2010: The Central Main Ethiopian Rift is younger than 8 Ma: confirmation through apatite fission-track thermo-chronology. *Terra Nova, 22,* 470–476.

Abebe, T., Manetti, P., Bonini, M., Corti, G., Innocenti, F., Mazzarini, F. and Pecksay, Z., 2005: *Geological map (scale 1:200,000) of the northern Main Ethiopian Rift and its implications for the volcano-tectonic evolution of the rift.* Geological Society of America, Map and Chart Series MCH094, 20 pp.

Abebe, Z., Sinetebeb, Y., and Eshetu, A., 2017: *Surface geothermal exploration mapping of Butajira-Selti area Ethiopia.* Geological Survey of Ethiopia GSE), unpublished report 1, 28 pp.

Acocella, V., Korme, T., and Salvini, F., 2003: Formation of normal faults along the axial zone of the Ethiopian rift. *J. Struct. Geol. 25,* 503-513.

Árnason K., 2006: TEMTD, *A programme for 1D inversion of central-loop TEM and MT data.* ISOR – Iceland GeoSurvey, short unpublished manual, 17 pp.

Árnason, K., Karlsdóttir, R., Eysteinsson, H., Flóvenz, Ó.G., and Gudlaugsson, S.Th., 2000: The resistivity structure of high-temperature geothermal systems in Iceland. *Proceedings of the World Geothermal Congress 2000, Kyushu-Tohoku, Japan,* 923-928.

Bigazzi, B., Bonadonna, F.P., Di Paola, G.M., and Giuliani, A., 1993: K-Ar and fission track ages of the last volcano-tectonic phase in the Ethiopian Rift Valley (Tulu Moye area). In: *Geology and Mineral resources of Somalia and Surrounding Regions. Instituto Agronomico Oltremare, Firenze, Relazioni Monografie 113,* 311–322.

Boccaletti, M., Bonini, M., Mazzuoli, R., Abebe, B., Picard, L., Tortorici, L., 1998: Quaternary oblique extensional tectonics in the Ethiopian Rift (Horn of Africa). *Tectonophysics, 287,* 97-116.

Bonini, M., Corti, G., Innocenti, F., Manetti, P., Mazzarini, F., Abebe, T. and Pecskay, Z., 2005: Evolution of the Main Ethiopian Rift in the frame of Afar and Kenya Rifts propagation. *Tectonics, 24, TC1007,* 25 pp.

Cagniard, L., 1953: Basic theory of the magnetotelluric method of geophysical prospecting. *Geophysics, 18,* 605-645.

Cantwell, T., 1960: *Detection and analysis of low frequency magnetotelluric signals.* MIT, Geology and Geophysics, Boston, PhD thesis, 170 pp.

Chernet, T., Hart, W.K., Aronson, J.L., and Walter, R.C., 1998: New age constraints on the timing of volcanism and tectonism in the northern Main Ethiopian Rift – southern Afar transition zone (Ethiopia). *J. Volcanol. Geotherm. Res. 80,* 267–280.

Di Paola, G.M., 1976: *Geological map of the Tullu Moje volcanic area, Arussi, Ethiopia Rift Valley.* Consiglio Nazionale delle Rieerehe, Italy, unpubl. report.

Ebinger, C.J. and Casey, M., 2001: Continental breakup in magmatic provinces, an Ethiopian example. *Geology, 29,* 527–530.

Ebinger, C.J., Yemane, T., Woldegabriel, G., Aronson, J.L. and Walter, R.C., 1993: Late Eocene – recent volcanism and faulting in the southern Main Ethiopian Rift. *J. Geological Society London, 150,* 99-108.

Eysteinsson, H., 1998: *TEMMAP and TEMCROSS plotting programs.* ÍSOR – Iceland GeoSurvey, unpublished programs and manuals.

Flóvenz, Ó.G., Hersir, G.P., Saemundsson, K., Ármannsson, H., and Fridriksson Th., 2012: Geothermal energy exploration techniques. In: Sayigh, A. (ed.), *Comprehensive renewable energy, vol 7.* Elsevier Oxford, United Kingdom, 51-95.

Flóvenz, Ó.G., Spangerberg, E., Kulenkampff, J., Árnason, K., Karlsdóttir, R., Huenges, E., 2005: The role of electrical interface conduction in geothermal exploration. *Proceeding of the World Geothermal Congress 2005, Antalya, Turkey,* 9 pp.

Gebrewold, Y., 2017: *Geothermal geochemistry of Butajira prospect area, Central Main Ethiopian Rift, implication for potential areas to geothermal energy in Ethiopia.* Geological Survey of Ethiopia (GSE), unpublished report.

George, R., and Rogers, N., 2002: Plume dynamics beneath the African plate inferred from the geochemistry of the Tertiary basalts of southern Ethiopia. *Contrib Mineral Petrol., 144-3,* 286-304.

Hayward, N.J. and Ebinger, C.J., 1996: Variations in the along-axis segmentation of the Afar Rift system. *Tectonics, 15,* 244-257.

Hersir, G.P., and Árnason K., 2009: Resistivity of rocks. *Paper presented at "Short Course on Surface Exploration for Geothermal Resources", organized by UNU-GTP and LaGeo, Santa Tecla, El Salvador,* UNU-GTP, SC-09, 8 pp.

Hofmann, C., Courtillot, V., Feraud, G., Rochette, P., Yirgu, G., Ketefo, E. and Pik, R. 1997: Timing of the Ethiopian flood basalt event and implications for plume birth and global change. *Nature*, 389, 838–841.

Hutchison, W., Mather, T.A., Pyle, D.M., Biggs, J., and Yirgu, G., 2015: Structural controls on fluid pathways in an active rift system: A case study of the Aluto volcanic complex. *Geosphere, 11-3,* 542–562.

Kazmin, V., Berhe. S.M., Nicoletti, M., and Pertucciani, C., 1980: Evolution of the northern part of the Ethiopian rift. *Atti Convegni Lincei*, *47,* 275-292.

Kebede, S., 2014: Geothermal exploration and development in Ethiopia: Country update report. *Papers presented at "Short course IX on Exploration for Geothermal Resources" organized by UNU-GTP, GDC and KenGen in Naivasha, Kenya,* UNU-GTP SC-19, 22 pp.

Keir, D., Ebinger, C.J., Stuart, G.W., Daly, E., and Ayele, A., 2006: Strain accommodation by magmatism and faulting as rifting proceeds to breakup: seismicity of the northern Ethiopian rift. *J. Geophysical Research, 111-B05314,* 17 pp.

Keller, G.V., and Frischknecht, F.C., 1966: *Electrical methods in geophysical prospecting*. Pergamon Press, NY, 527 pp.

Lahitte, P., Gillot, P.Y., and Courtillot, V., 2003: Silicic central volcanoes as precursors to rift propagation: the Afar case. *Earth Planet. Sci. Lett*., *207*, 103-116.

Le Turdu, C., Tiercelin, J.J., Gibert, E., Travi, Y., Lezzar, K.E., Richert, J.P., Massault, M., Gasse, F., Bonnefille, R., Decobert, M., Gensous, B., Jeudy, V., Tamrat, E., Mohammed, M.U., Martens, K., Atnafu, B., Cherent, T., Williamson, D., Taieb, M., 1999: The Ziway-Shala Lake basin system, Main Ethiopian Rift: Influence of volcanism, tectonics and climatic forcing on basin formation and sedimentation. *Palaeogeogr. Palaeoclimatol. Palaeoecol., 150,* 135-177.

Lemma Didana Y., 2010: *Multidimensional inversion of MT data from Krýsuvík high-temperature geothermal field, SW-Iceland, and study of how 1D and 2D inversion can reproduce a given 2D/3D resistivity structure using synthetic MT data*. University of Iceland, MSc thesis, UNU-GTP, Iceland, report 4, 94 pp.

Levitte, D., Columba, J, and Mohr, P., 1974: Reconnaissance geology of the Amaro Horst, South Ethiopia rift. *Geological Society of America - Bulletin, 85,* 417-422.

Mohr, P.A., 1962: The Ethiopian Rift System. *Bull. Geophys. Obs., Addis Ababa University 5,* 33-62.

Mohr, P.A., 1971: Ethiopian rift and plateaus: some volcanic petrochemical differences*. J. Geophys. Res. 76-8,* 1967– 1983.

Mohr, P. A., 1983: Volcano tectonic aspects of the Ethiopian Rift evolution. *Bull. Cent. Rech. Explor. Prod. Elf Aquitaine, 7,* 175-189.

Molin, P., and Corti, G., 2015: Topography, river network and recent fault activity at the margins of the central Main Ethiopian Rift. *Tectonophysics, 664,* 67-82.

Parkinson, W.D., 1959: Direction of rapid geomagnetic fluctuations. *Geophysic. J.R. Astron. Soc.,* 2, 1-14.

Phoenix Geophysics, 2005*: Data processing. User guides*. Phoenix Geophysics, Ltd., Toronto. Press Ltd., Oxford, 527 pp.

Pik, R., Deniel, C., Coulon, G., Hofmann, C., and Ayalew, D., 1998: The northwestern Ethiopia plateau flood basalts. Classification and spatial distribution of magma types. *J. Volcanol., Geotherm, Res, 81,* 91-111.

Pizzi, A., Coltorti, M., Abebe, B., Disperati, L., Sacchi, G., and Salvini, R., 2006: Wonji fault belt (Main Ethiopian Rift): structural and geomorphological constraints and GPS monitoring. The Afar Volcanic Province within the East African Rift System. *Geological Society, London, Special Publications*, 259, 191–207.

Seifemichael, B., and Kazmin, V., 1978: *Geology and development of the Nazret area.* Ministry of Mines, Ethiopian Geol. Survey, Addis Ababa, Note. 100.

Tadesse, T., 2018: Appendices to the report: 1D inversion of magnetotelluric data from Ashute, Butajira geothermal prospect, SE-Ethiopia and its geothermal implications. UNU-GTP, Iceland, report 29 appendices, 70 pp.

Tikhonov, A.N., 1950: The determination of electrical properties of the deep layers of the earth´s crust (in Russian). *Dokl. Acad. Nauk. SSR, 73*, 295-297.

Ukstins, I.A., Renne, P.R., Wolfenden, E., Baker, J., Ayalew, D., and Menzies, M., 2002: Matching conjugate rifted margins 40 Ar/39 Ar chrono-stratigraphy of pre- and syn-reft bimodal flood volcanism in Ethiopia and Yemen. *Earth and Planetary Science Letters, 198*, 289-306.

UNDP, 1973: *Geology, geochemistry and hydrology of hot springs of the East African Rift System within Ethiopia*. UNDP, December report DD/SF/ON/11, NY.

Vozoff, K., 1972: The magnetotelluric method in the exploration of sedimentary basins: *Geophysics, 37*, 980-1041.

Vozoff, K., 1991: The magnetotelluric method. In: Nabighian, M.N. (ed*.), Electromagnetic methods in applied geophysics, vol. 2B.* Society of Exploration Geophysicists, Tulsa, OK, 641-711.

Wiese, H., 1962: Geomagnetische Tiefentellurik, Teil 2, Die Streichrichtung der Untergrundstrukturen des elektrischen Winderstandes, ersclossen aus geomagnetischen Variationen (in German). *Geofis. Pura. Appl., 52*, 83-103.

Woldegabriel, G., Aronson, J.L., and Walter, R.C., 1990: Geology geochronology and rift basin development in the central sector of the Main Ethiopian Rift. *Geol. Soc. Am. Bull., 102,* 439-458.

Woldegabriel, G., White, T., Suwa, G., Semaw, S., Beyene, Y., Asfaw, B., Walter, R., 1992: Kessem-kebena: a newly discovered paleoanthropological research area in Ethiopia. *J. Field Archeol., 19,* 471-493.

Wolfenden, E., Ebinger, C., Yirgu, G., Deino, A., Ayalew, D., 2004: Evolution of the northern Main Ethiopian Rift: birth of a triple junction. *Earth Planet. Sci. Lett., 224*, 213-228.

Zanettin, B., Justin-Visentin, E., Nicoletti, M., and Petrucciani, C., 1978: Evolution of the Chencha escarpment and the Ganjiuli graben (Lake Abaya) in the Southern Ethiopian rift*, Nues. Jahrb. Geol. Paleontol. Monatsh, 8,* 473-490.